HHS Public Access

Author manuscript

Immunity. Author manuscript; available in PMC 2024 July 11.

Published in final edited form as:

Immunity. 2023 July 11; 56(7): 1533–1547.e7. doi:10.1016/j.immuni.2023.06.001.

Lipids regulate peripheral serotonin release via gut CD1d

Jialie Luo[1,4], **Zuojia Chen**[1,4], **David Castellano**[2], **Bin Bao**[3], **Wenyan Han**[2], **Jian Li**[1], **Girak Kim**[1], **Dingding An**[3], **Wei Lu**[2], **Chuan Wu**[1,5]

[1]Experimental Immunology Branch, National Cancer Institute, NIH, Bethesda, MD, USA

[2]Synapse and Neural Circuit Research Section, National Institute of Neurological Disorders and Stroke, NIH, Bethesda, MD, USA

[3]Department of Pediatrics, Boston Children's Hospital, Harvard Medical School, Boston, MA, USA

[4]These authors contributed equally to this work

[5]Lead contact

Summary

The crosstalk between the immune and the neuroendocrine system is critical for intestinal homeostasis and gut-brain communications. However, it remains unclear how immune cells participate in gut sensation of hormones and neurotransmitters release in response to environmental cues, such as self and microbial lipids. We show here that lipid-mediated engagement of invariant natural killer T (iNKT) cells with enterochromaffin (EC) cells, a subset of intestinal epithelial cells, promoted peripheral serotonin (5-HT) release via a CD1d-dependent manner, regulating gut motility and hemostasis. We also demonstrated that inhibitory sphingolipids from symbiotic microbe *Bacteroides fragilis* represses 5-HT release. Mechanistically, CD1d ligation on EC cells transduced a signal and restrained potassium conductance through activation of protein tyrosine kinase Pyk2, leading to calcium influx and 5-HT secretion. Together, our data reveal that by engaging with iNKT cells, gut chemosensory cells selectively perceive lipid antigens via CD1d to control 5-HT release, modulating intestinal and systemic homeostasis.

Graphical Abstract

Correspondence: Chuan Wu (chuan.wu@nih.gov).

Authors' contribution

J.Luo, Z.C., and C.W. planned and conceptualized the paper; J.Luo., Z.C., D.C., B.B., W.H., J.Li and G.K. conducted experimentation and data analysis; D.A. and W.L provided key resources; J.Luo, Z.C. and C.W. wrote and edited the manuscript; C.W. provided supervision.

Declaration of interests

The authors declare no competing interests.

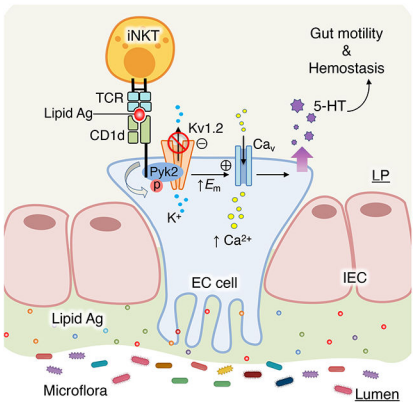

Enterochromaffin (EC) cells are known as the major source of gut-derived serotonin (5-HT). Luo et al. demonstrate that lipid-mediated engagement of invariant natural killer T (iNKT) cells with EC cells regulates peripheral 5-HT release via a CD1d-dependent manner, indicating an immunemediated selective neuroendocrine response to lipid antigens.

Introduction

Intercellular interactions are recognized to be critical for the maintenance of barrier integrity, particularly at the intestinal mucosal surface of the epithelium. The involvement of various gut microbiota introduces one more dimension for such interactions on the barrier interface. As a major endocrine organ, different enteric endocrine cells are dispersed within the intestinal epithelial cells (IECs), converting different stimuli from surrounding cells and luminal microbes into chemical signals to regulate intestinal physiology.[1] One subset of enteric endocrine epithelial cells is enterochromaffin (EC) cells, which is known as the major source of gut-derived serotonin (5-hydroxytryptamine (5-HT)).[2,3] 5-HT is a critical enteric hormone that exerts a broad spectrum of functions to control both intestinal and systemic physiology. Within the gastrointestinal (GI) tract, 5-HT is involved in gut motility, secretion and sensation.[4–6] Gut-derived 5-HT is also known to influence extraintestinal compartments, regulating cardiac function, hemostasis, metabolism, and bone development.[7–11]

Given that EC cells reside within the gut epithelium where a variety of immune cells can be found, it is highly possible that immune cells contribute to EC cell homeostasis and activation by direct interactions. Previous studies have demonstrated that T cells regulate EC cell expansion to enhanced 5-HT amounts during enteric infection, suggesting the important role of immune responses for EC cell biology in the gut.[12,13] In addition, immune regulators such as cytokines, have also been documented to trigger either expansion or activation of EC cells for intestinal homeostasis or inflammation.[14,15] Given the variety of immune cells with different properties, detailed investigation to understand the role of an immune-neuroendocrine axis for local and systemic physiology and pathophysiology is necessary.

Invariant natural killer T (iNKT) cells are known as a rare subset of T cells which recognize CD1d-restricted self and microbial lipid antigens for immune homeostasis and

host defenses.[16,17] Previous studies suggest that the context of a lipid determines the outcome of iNKT cell responses.[18–20] For instance, in addition to endogenous lipid antigens which induce iNKT cell activation and expansion, microbial inhibitory sphingolipids have been demonstrated to negatively regulate iNKT cell homeostasis.[20] The presence of iNKT cell in the GI tract has been associated with epithelium development and intestinal barrier integrity.[21,22] On the other hand, CD1d is an MHC class I–related protein that is found to be constitutively expressed on intestinal epithelial cells (IECs).[23–25] CD1d plays a key role in presenting glycolipid antigens to iNKT cells, leading to iNKT cell activation and cytokine release.[26,27] Within the GI tract, IECs have been suggested to present lipid antigens to iNKT cells during infection, initiating anti-microbial defense.[28,29] Meanwhile, the engagement of iNKT cells and antigen presenting cells (APCs) can also conversely regulate diverse APC functions via CD1d, including both professional (dendritic cells) and unconventional (IECs) APCs.[21,30] Although it has been illustrated that within the GI tract, crosslinked CD1d on IECs leads to IL-10 production for anti-inflammatory responses,[30] a understanding of how such engagements modulate intestinal homeostasis is still not complete.

Here we reveal an unexpected role of iNKT-EC cell interactions in regulating intestinal 5-HT release, impacting both intestinal and systemic homeostasis. Loss of iNKT cells or deletion of CD1d in EC cells resulted in compromised peripheral 5-HT release. Supplementation of conventional lipid antigen induced rapid release of 5-HT by CD1d engagement on EC cells with iNKT cells. Mechanistically, we demonstrated that lipid-mediated CD1d-ligation on EC cells induces proline-rich tyrosine kinase 2 (Pyk2) activation, which in turn regulates voltage-gated potassium channel subfamily A member 2 (Kvl.2) by tyrosine phosphorylation. Additionally, single EC cell electrophysiology studies uncovered that CD1d signaling restrained K^+-conductance in a Pyk2 dependent manner, promoting Ca^{2+} influx and 5-HT release. Finally, in addition to conventional lipid antigens, we demonstrated that inhibitory sphingolipids from microbe *Bacteroides fragilis* repressed 5-HT amounts *in vivo*. Therefore, our data elucidate a previously unappreciated role of iNKT-EC cell crosstalk in calibrating intestinal neuroendocrinal responses, revealing a gatekeeping mechanism that the immune system collaborates with the nervous system to selectively respond to environmental cues of lipid antigens.

Results

iNKT cell regulates gut motility

During intestinal inflammation, immune responses often lead to noxious substances elimination by activating peristalsis or diarrhea.[31] To understand whether iNKT cells are capable in regulating intestinal peristalsis, we carried out a murine oxazolone colitis model mediated by iNKT cells for human ulcerative colitis (UC).[32–34] Indeed, we observed enhanced iNKT cell infiltration during inflammation (Figures S1A–S1D), associated with elevated colonic tissue contraction in oxazolone-treated mice compared to ethanol-treated control mice (Figures S1E–S1H). Hence, our data suggest that in addition to cytokine production for host defense and immune homeostasis, iNKT cell may also be involved in controlling gut motility.

In response to lipid antigens, iNKT cells are rapidly activated and release various of cytokines.[35] To further assess the role of iNKT cells in gut motility, we administered synthetic glycolipid KRN7000 (α-GalCer) by daily intraperitoneal (i.p.) injection for a week and observed decreased colonic transit time compared to those treated with PBS (Figure 1A), indicating that lipid-mediated iNKT cell activation influenced gut motility. Meanwhile, we employed *Cd1d*$^{-/-}$ and *Traj18*$^{-/-}$ mice, which are known to lack in iNKT cells,[36,37] and found that both mouse strains displayed prolonged intestinal transit time compared to WT controls (Figures 1B and S2A). Colonic tissues from *Cd1d*$^{-/-}$ and *Traj18*$^{-/-}$ mice exhibited impaired peristaltic contraction compared to WT mice (Figures 1C and S2B). Moreover, while lipid antigen promoted gut motility in WT mice, this effect was abolished in either *Cd1d*$^{-/-}$ or *Traj18*$^{-/-}$ mice after a week of treatment with α-GalCer (Figures S2C and S2D), indicating that both CD1d-expressing APCs and iNKT cells were critical for the lipid-mediated gut motility. We then evaluated how rapidly lipids modulate intestinal peristalsis. By testing different intermediate time points, we found a shortened colonic transit time of 10 min after α-GalCer administration (Figures 1D and 1E). We also noticed that α -GalCer induced rapid colonic tissue contraction in WT mice but not in *Cd1d*$^{-/-}$ or *Traj18*$^{-/-}$ mice (Figure 1F). Collectively, these data suggest that lipid promotes instantaneous peristaltic movement that requires iNKT cells.

IEC-derived CD1d is required for gut motility

The engagement of iNKT cells and CD1d-expressing APCs leads to rapid iNKT cell activation and cytokine release,[38] which could potentially impact gut motility. Meanwhile, within the GI tract, CD1d can be found on dendritic cells (DCs) and IECs which plays a critical role for gut immune homeostasis.[21] To our surprise, we found that IEC-derived CD1d (*Vil1*^{cre}*Cd1d1*$^{fl/fl}$) specifically influenced intestinal peristalsis (Figures S2E and 2A). Indeed, loss of CD1d in IECs impaired intestinal transit time (Figures 2B and S2F), accompanied by diminished α-GalCer-induced rapid colonic contractive response (Figures S2G, S2H, 2B and 2C), suggesting that iNKT cell activation was dispensable for gut motility. By using *Pirt*^{GCaMP3} mice, which carry a calcium indicator for enteric neuronal activities,[39] we noticed elevated neuronal activity in the myenteric plexus when we treated isolated colonic tissue with α-GalCer (Figure 2D). Importantly, removal of the epithelium layer from the colonic tissues abolished α-GalCer-mediated neuronal responses (Figures 2E–2G), indicating that IEC-derived CD1d was essential in mediating lipid antigeninduced gut motility by activating enteric neurons.

Lipids induce 5-HT secretion from EC cells for gut motility

Our previous studies demonstrates that immune stimulation promotes EC cell-derived 5-HT release, leading to activation of enteric neurons and gut motility.[15,40] Based on this lead, we found rapid increase of serum 5-HT after α-GalCer administration (Figure 3A), indicating that lipid promoted 5-HT release. Consistently, we found reduced serum 5-HT amouts in both *Traj18*$^{-/-}$ and *Vil1*^{cre}*Cd1d*$^{fl/fl}$ mice compared to their control mice (Figures 3B and 3C), suggesting that the interactions between IEC and iNKT cells were critical for 5-HT release. To confirm the role of 5-HT in lipid-mediated gut motility, we utilized *Vil1*^{cre}*Tph1*$^{fl/fl}$ mice, in which gut-derived 5-HT biosynthesis is impaired.[15,41] With addition of α-GalCer-enhanced peripheral 5-HT in WT mice, this effect was completely

abolished in *Vil1*^{cre}*Tph1*$^{fl/fl}$ mice (Figure 3D). Moreover, *Vil1*^{cre}*Tph1*$^{fl/fl}$ mice displayed delayed intestinal transit time compared to *Tph1*$^{fl/fl}$ control mice (Figures 3E and S3A), and α-GalCer-induced gut motility was 5-HT dependent (Figures 3E and 3F). We also found that colon tissues displayed impaired peristaltic contraction after treatment of $5HT_3$ receptor ($5HT_3R$) antagonist. Moreover, additional α-GalCer did not rescue the phenotype (Figures S3B and S3C), suggesting that $5HT_3Rs$ dominantly contribute to lipid-mediated gut motility.

It is well established that EC cells generate the major body of peripheral 5-HT.[3,42] By using *Chga*$^{cre\text{ER}}$ mice to selective target EC cells,[15] we further investigated the role of CD1d on EC cells for 5-HT release (Figure S3D). *Chga*$^{cre\text{ER}}$*Cd1d1*$^{fl/fl}$ mice exhibited normal amounts of EC cells and 5-HT biosynthesis gene expression in colonic tissues as compared to control mice (Figures S3E–S3G). Although *Chga*$^{cre\text{ER}}$*Cd1d1*$^{fl/fl}$ mice displayed no change in iNKT cells (Figures S3H–S3J), loss of CD1d in EC cells led to impaired serum 5-HT amouts and colonic contractibility (Figures 3G, S3K and S3L). Importantly, while supplementation of α-GalCer elevated 5-HT in control mice, it failed to induce 5-HT in *Chga*$^{cre\text{ER}}$*Cd1d1*$^{fl/fl}$ mice (Figure 3G). Consequently, CD1d deficiency in EC cells resulted in impaired gut motility induced by α-GalCer compared to the control mice (Figures 3H, 3I and S3M). Collectively, these findings indicate that engagement of lipid antigens with CD1d in EC cells induced rapid 5-HT release, subsequently promoting intestinal peristalsis.

Lipid-mediated 5-HT release rapidly enhances platelet function for hemostasis

It has previously shown that gut-derived 5-HT in the periphery is mainly taken up by platelets for their activation at sites of injury sites to promote hemostasis.[40,43,44] We next investigated whether iNKT cells are required for 5-HT-mediated platelet activation and hemostasis. We noticed that *Traj18*$^{-/-}$ mice displayed prolonged bleeding time with normal platelet counts compared to WT mice (Figures S4A and S4B). Further, we found less activated platelets from *Traj18*$^{-/-}$ mice compared to WT mice, as measured by the activation markers CD62P (P-selectin) and Jon/A (CD41 and CD61) (Figures S4C and S4D), suggesting that iNKT cells contributed to platelet activation during blood clotting. Similarly, we found prolonged bleeding time associated with compromised platelet activities in *Chga*$^{cre\text{ER}}$*Cd1d1*$^{fl/fl}$ mice, but unchanged platelet counts compared to control mice (Figures S4E–S4H). Lastly, we also showed that no CD1d was found on platelets, that did not respond to α-GalCer activation directly (Figures S4I–S4K), excluding the direct effect of lipid antigen on platelets. Together, these data indicate that EC cellrestricted CD1d signal was important for platelet activation.

Platelets are activated via the uptake of 5-HT in a short time.[40,45] We noticed elevated platelet activity in WT mice but not *Traj18*$^{-/-}$ or *Chga*$^{cre\text{ER}}$*Cd1d1*$^{fl/fl}$ mice 10 min after α-GalCer injection (Figures 4A–4F), suggesting that lipid-mediated platelet activity depended on iNKT and EC cells. Consequently, we found that α-GalCer supplement improved hemostasis in WT mice, while this effect was diminished in both *Traj18*$^{-/-}$ and *Chga*$^{cre\text{ER}}$*Cd1d1*$^{fl/fl}$ mice (Figures 4G and 4H). To address whether lipid antigen-mediated hemostasis depends on 5-HT, we employed *Vil1*^{cre}*Tph1*$^{fl/fl}$ mice and observed that α-GalCer administration did not alter platelet activity in *Vil1*^{cre}*Tph1*$^{fl/fl}$ mice (Figures 4I and 4J). Accordingly, α-GalCer injection did not shorten bleeding time in *Vil1*^{cre}*Tph1*$^{fl/fl}$ mice

(Figure 4K), indicating that 5-HT was essential for lipid-mediated hemostasis. Collectively, our data suggest that lipid promotes EC cell-derived CD1d ligation for 5-HT release, resulting in a rapid platelet activation for hemostasis.

CD1d signal intrinsically modulates 5-HT release from EC cells

To directly measure EC cell activation for 5-HT release, we disassociated EC cells from the intestine of *Tph1*^{CFP} mice. We positioned iNKT cells purified from V α14-J α18 transgenic (*Va14* Tg) mice[46] in contact with EC cells and monitored stimulus-evoked changes in cytoplasmic Ca^{2+} simultaneously in CFP^+ EC cells and adjacent biosensor cells with a 5-HT-gated ion channel ($5HT_3R$) (Figure 5A). We observed robust α-GalCerevoked Ca^{2+} responses in WT EC cells when they were in contact with iNKT cells, followed by Ca^{2+} influx in adjacent biosensor cells (Figure 5B). Additionally, extracellular K^+-mediated EC cell depolarization induced Ca^{2+} responses in both EC and biosensor cells, while $5\text{-}HT_3R$ agonist mCPBG evoked a Ca^{2+} response in biosensor cells but not EC cells (Figure 5B). Absence of iNKT cells in the system completely abolished α-GalCer-induced Ca^{2+} responses from both EC cells and biosensor cells (Figures S5A, 5C–5E). Consistently, we found enhanced interactions between iNKT cells and $5\text{-}HT^+$ EC cells in the colonic tissue from oxazolone treated mice compared with naïve mice (Figures S5B and S5C). Further, we found elevated peripheral 5-HT amounts during intestinal inflammation compared to mice under steady state (Figure S5D). Thus, there is a positive correlation between the iNKT-EC cell interactions and 5-HT production. Altogether, these data demonstrate that iNKT cells enable EC cell activation for 5-HT release.

To discriminate whether CD1d-mediated EC cell activation occurs via cell intrinsic or extrinsic mechanisms, we collected the supernatant from *in vitro* cultured activated iNKT cells and examined its effect for gut motility. Both *in vivo* and *in vitro* tests showed no changes in gut motility, indicating that CD1d probably exerted its function for 5-HT release through cell intrinsic machinery (Figures S5E and S5F). Further, we isolated single EC cells from *Tph1*^{CFP} mice loaded with or without cell tracker Far Red to distinguish WT from *Cd1d*$^{-/-}$ EC cells (Figure 5F). We positioned WT and *Cd1d*$^{-/-}$ EC cells simultaneously in contact with iNKT cells and found that α-GalCer induced robust Ca^{2+} influx in WT but not *Cd1d*$^{-/-}$ EC cells, while both cells responded to extracellular K^+ (Figures 5G and 5H). Given that TCR-CD1d interactions activate iNKT cells for cytokine release,[35,47] our data demonstrate that CD1d-mediated EC cell activation was through a cell intrinsic mechanism. Finally, we isolated single EC cells from *Cd1d*$^{-/-}$*Tph1*^{CFP} intestinal organoids lentivirally overexpressing full-length (WT LV) or intracellular domain truncated CD1d (*CD1d*$^{\Delta}$ LV) (Figures S5G and 5I). We observed that α-GalCer induced Ca^{2+} influx in WT LV but not *CD1d*$^{\Delta}$ LV EC cells, indicating that CD1d intracellular tail contributed to EC cell activation (Figures 5J and 5K).

Pyk2-Kv1.2 axis is required for CD1d-mediated EC cell activation

A previous study showed that CD1d signaling induces Tyr332 phosphorylation of the CD1d intracellular domain, resulting in recruitment and activation of Pyk2.[48] Indeed, by stimulating human EC cell line BON-1 with crosslinked anti-CD1d, we found enhanced phosphorylated Pyk2 (p-Pyk2) signal, accompanied with elevated 5-HT secretion (Figures

6A and S6A). We also observed enhanced p-Pyk2 in primary EC cell-enriched murine intestinal organoids stimulated with crosslinked anti-CD1d (Figure 6B), indicating that Pyk2 acted as a downstream signal of CD1d. Consistently, we observed that α-GalCerevoked Ca^{2+} responses in WT EC cells in contact with iNKT cells were largely diminished in the presence of p-Pyk2 inhibitor PF-431396 (Figures 6C and 6D). While we showed CD1d intracellular domain might be required for EC cell activation, it is also possible that cytoplasmic tail truncation affects CD1d recycling,[49] which in turn impairs antigen capture instead of intracellular signaling. To this end, we lentivirally overexpressed CD1d intracellular domain with Tyr332 phosphorylation mutation (*CD1d*^{Y332A}) in *Cd1d*$^{-/-}$ *Tph1*^{CFP} EC cells and found ablated α-GalCer-induced Ca^{2+} influx compared to WT LV cells (Figures 6E and 6F). These data suggest that CD1d intracellular tail is essential for EC cell activation which depended on CD1d Tyr332-mediated recruitment and activation of Pyk2.

It has been reported that Pyk2 activation inhibits K^+ currents due to tyrosine phosphorylation of Kv1.2.[50,51] Inhibition of Kv1.2 results in opening of voltage gated Ca^{2+} channels.[50] Therefore, we hypothesized that CD1d-mediated activation of Pyk2 results in repression of the Kv1.2 channel and an increased Ca^{2+} influx in EC cells for 5-HT release. Indeed, we detected that Kv1.2 was expressed on intestinal EC cells (Figure 6G). To investigate whether the CD1d signal impacted Kv1.2 function, we performed coimmunoprecipitation on BON-1 cells and found that phosphorylated tyrosine was detected on both Pyk2 and Kv1.2 upon CD1d activation, while this modification was abolished with PF-431396 treatment (Figure 6H). Given the proximity between CD1d and Kv1.2 (Figure 6I), our data indicate that CD1d-induced Pyk2 activation in turn regulated Kv1.2 channel by tyrosine phosphorylation.

To further address the functional alteration of Kv1.2 on EC cells upon CD1d activation, we carried out single EC cell electrophysiology studies on primary EC cells. Whole-cell patch-clamp recordings showed that, in response to a series of voltage steps, outward currents were reduced in the presence of TsTx-Kα, a selective blocker for Kv1.2 subunits,[52] followed by a further reduction in the presence of tetraethylammonium (TEA, a potassium channel blocker) (Figures S6B–S6E). Plus, TsTx-Kα treatment induced Ca^{2+} responses from both EC cells and 5-HT_3R biosensor cells (Figure S6F) and enhanced 5-HT release from BON-1 cells (Figure S6G). Together, these data suggest functional surface expression of Kv1.2 channels in EC cells is required for 5-HT release.

To determine whether iNKT cell activation influences EC cell K^+-conductance, EC cells were first patched in cell-attached configuration and brought into contact with iNKT cells (Figure S6H). Following a series of voltage steps, outward currents were observed in EC cells that were subsequently reduced after α-GalCer application compared to control wash (Figures 6J and 6K). In response to a +100 mV depolarizing step, there was a reduction in the current amplitude (Figure 6L). However, PF-431396 treatment abolished this difference of the outward currents between control and α-GalCer solutions (Figures 6M–6O). Collectively, these findings demonstrate that lipid antigen-mediated CD1d signaling restrain EC cell K^+-conductance in a Pyk2 dependent manner, leading to Ca^{2+} influx and 5-HT release (Figure S6I).

Bacteroides fragilis sphingolipids repress intestinal 5-HT secretion

Recent studies highlight a role for the microbiota in regulating peripheral 5-HT amount.[53,54] However, it is unclear whether specific bacterial products, such as sphingolipids contribute to host 5-HT amount. Bacterial sphingolipids have been reported to act as a negative regulator for iNKT cell expansion.[20] To further understand if lipids control the iNKT-EC cell axis for 5-HT release, we carried out a mono-colonized mouse model of symbiotic microbe *B. fragilis* as previously described.[20] It has been shown that *B. fragilis* has a homolog of the host gene that encodes serine palmitoyltransferase (SPT), the enzyme in the eukaryotic sphingolipid biosynthetic pathway. Deleting this bacterial homolog renders the *B. fragilis* mutant (called ΔSPT) unable to produce sphingolipids.[20,55] Using monocolonized WT (BFWT) or mutant *B. fragilis* (BFΔSPT) mice, we confirmed enhanced colonic iNKT cells in BFΔSPT mice as previously described (Figures S7A–S7C). Further, we noticed that BFΔSPT mice exhibited comparable EC cells (Figures S7D and S7E) and 5-HT biosynthesis gene expression (Figure S7F) compared to BFWT mice. Importantly, monocolonizing BFΔSPT led to elevated serum 5-HT amount (Figure 7A). We also noticed that BFΔSPT mice exhibited enhanced intestinal peristalsis compared to BFWT mice (Figures 7B and S7G). Moreover, we found that BFΔSPT mice displayed shortened bleed time with normal platelet counts compared to BFWT mice (Figures 7C and S7H). Enhanced platelet activation was observed in BFΔSPT mice compared to control mice (Figures 7D and 7E).

Moreover, we assessed the effect of inhibitory component in *B. fragilis* sphingolipids, GSL-Bf717,[20] upon 5-HT release. We found that GSL-Bf717 exhibited an antagonistic effect to α-GalCer-mediated rapid 5-HT release (Figure 7F). Accordingly, we observed similar inhibitory effect of GSL-Bf717 on gut motility and hemostasis (Figures 7G and 7H). Moreover, we noticed that α-GalCer-induced Ca^{2+} responses in WT EC cells were largely abolished in the presence of inhibitory lipid GSL-Bf717 (Figures 7I and 7J), suggesting that GSL-Bf717 block EC cell-mediated 5-HT release as opposed to α-GalCer.

Discussion

The intestinal epithelium acts as the frontier of host defense and plays a critical role not only in innate immune responses, but also in gut sensation.[1] EC cells within the intestinal epithelium are known to function as a chemosensors, converting the environmental stimuli into 5-HT for neuroendocrinal responses.[56] While it has been suggested that immune cells modulate EC cell activation and function, such crosstalk mostly occurs via secretory mediators such as cytokines.[12,14,15] Our current work demonstrated a direct interaction between iNKT cells and EC cells via CD1d that controls EC cell activation and 5-HT secretion, consequently regulating the intestinal peristalsis and hemostasis. We further showed that CD1d ligation triggers Ca^{2+} influx for 5-HT release via a Pyk2-Kv1.2 signaling cascade.

In both animal models and human patients with intestinal inflammation, extracellular and circulating 5-HT amounts are increased.[57–59] 5-HT has also been identified to play a pathogenic role during experimental colitis.[60] While the underlying mechanisms regarding how 5-HT is involved in inflammatory colitis is still unclear, our data suggest that intestinal inflammation-mediated iNKT cell recruitment and expansion contribute to 5-

HT enhancement via CD1d crosslink on EC cells. Besides the EC cells, many immune cells, including mast cells, ILCs, and T cells, have been reported to express Tph1 and 5-HT.[61–63] While our current work specifically focused on EC cell by utilizing *Vil1*^{cre}*Tph1*$^{fl/fl}$ and *Chga*^{creER}*Cd1d1*$^{fl/fl}$ mice, the contribution of other 5-HT producing cellular sources warrants future studies. On the other hand, intestinal inflammation results in iNKT cell activation and expansion by glycolipid antigens for effector cytokine release. In particular, iNKT cell-derived IL-13 plays a critical role for the development of colitis.[32] During intestinal type 2 immune responses, IL-13 promotes EC cell hyperplasia, leading to elevated 5-HT production,[14] suggesting that iNKT cell could modulate EC cell expansion and 5-HT amouts via its cytokine production. Thus, our findings complement these previous studies and illustrate that the iNKT cell exerts dual roles in both EC cell expansion and a rapid neural EC cell response of 5-HT release. However, we note that while oxazolone-induced mouse colitis mimics many features of UC in humans,[32,33,64] it still requires further investigation to validate the precise role of iNKT cells in IBD patients.

iNKT cells are known as a rare population of immune cells in the gut that are involved in bacterial-host symbiosis.[22] Previous studies showed that CD1d plays a critical role in bacterial colonization in the intestine. Both IECs and immune cells are involved in regulating commensalism via CD1d-meditated presentation of intestinal lipids.[21,22] Consequently, CD1d deficiency-mediated dysbiosis results in enhanced susceptibility of intestinal inflammation.[65] Moreover, 5-HT is known to participate in regulation of microbiota composition for intestinal physiology,[66] suggesting an alternative role for CD1d in controlling gut commensalism via impacting 5-HT release from EC cells. The gut microbiota has also been shown to control host 5-HT biosynthesis, modulating peripheral 5-HT amouts.[67] Our inducible CD1d deletion animal model suggests that, in addition to CD1d-derived commensalism for 5-HT regulation, CD1d can also directly control EC cell function of 5-HT secretion. Hence, we show here that CD1d controls mucosal 5-HT amounts via both microbiota extrinsic and EC cell intrinsic mechanisms.

CD1d signal induces IL-10 production from IECs via a STAT3 dependent manner.[30] Meanwhile, CD1d ligation also promotes degranulation of lysosome from Paneth cells,[22] which is mediated via a Ca^{2+} dependent machinery.[68,69] Our findings indicate that iNKT cell-mediated CD1d ligation on EC cells regulates rapid 5-HT release, which is also governed by Ca^{2+} influx.[70] Therefore, crosslink of CD1d could lead to different outcomes from IECs via either transcriptional regulation or transient neuroendocrine responses, depending on cellular properties of different IEC subsets. Moreover, CD1d plays a key role in a murine model for UC.[32,71] Consistent with the animal studies, IBD patients were found to exhibit enriched intestinal CD1d-restricted NKT cells.[28,72] Additionally, intestinal iNKT cells possess both pro- and anti-inflammatory properties, which can be differentially controlled by distinct CD1d expressing cells.[21,30,73] While it is still unclear the molecular mechanism by which the engagement of TCR and CD1d through specific antigen presenting cells determines iNKT cell function, it is possible that different characteristics of glycolipids contribute to the outcome of intestinal inflammation.

Pyk2 has been reported to be mainly expressed in neurons in the central nervous system and plays a critical role in various neurological disorders.[74] Activation of Pyk2 is known to

be controlled by intracellular Ca^{2+} in neurons.[50] Since we show that CD1d-mediated Pyk2 activation leads to repression of Kv1.2 and enhancement of Ca^{2+} influx, the extracellular Ca^{2+} influx could further amplify Pyk2 activation, forming a positive feedback loop and an autoregulatory role for EC cell activation. On the other hand, Pyk2 is known as a potential causal gene for UC.[75] Inhibition of Pyk2 phosphorylation reduces intestinal inflammation by targeting pro-inflammatory macrophage.[76] Considering abnormally elevated 5-HT is observed in a range of gastrointestinal disorders,[77,78] Pyk2 could be a potential target for intervention of IBD associated disorders, like irritable bowel syndrome (IBS) with diarrhea.

While different components within *B. fragilis* sphingolipids exhibit distinct effects in regulating iNKT cells,[20,55,79] the whole *B. fragilis* has been shown to antagonize iNKT cell function and suppress colonic NKT cell proliferation.[20] Thus, GSL-Bf717 represents an inhibitory property of *B. fragilis* sphingolipids, which is functionally opposite to the sphingolipids produced by pathobiont *Sphingomonas* species[80] or sponge-derived α-GalCer. However, the specific mechanism of GSL-Bf717 in regulating EC cell activation is still unclear. It is possible that GSL-Bf717 functions as an antagonistic ligand or takes up the CD1d binding pocket with high affinity. Alternatively, GSL-Bf717 could suppress EC cell activation by interfering other surface proteins that mediate cell-cell interactions or local cytokine release. Therefore, although *B. fragilis* glycosphingolipids and α-GalCer have opposing effects on EC cell activation, we cannot rule out the possibilities that GSL-Bf717 represses 5-HT release via other mechanisms than directly inhibiting CD1d signaling.

Together, we have shown that EC-derived CD1d regulates the 5-HT release mediated by lipid antigens for both local gut motility and systemic hemostasis. In addition to their function in anti-microbial defense, iNKT cells conduct signal via CD1d ligation in EC cells to regulate peripheral hormone homeostasis. Furthermore, we elucidate that iNKT cells facilitate the selective ligation of CD1d via lipid antigens to transduce CD1d signal upon EC cells for 5-HT release, shedding light on how immune system and nervous system collaborate for host defense. Our findings thus provide alternative approaches for 5-HT related disorders by manipulation of CD1d or supplement of regulatory lipid antigens.

Limitations of the study

We show that Pyk2 activation induces Kv1.2 channel repression. However, to directly demonstrate that Pyk2-mediated Kv1.2 phosphorylation results in EC cell activation and 5-HT release, we need to identify and mutate Kv1.2 intracellular Tyr332 phosphorylation sites. We can then perform the whole-cell patch-clamp recordings on EC cell with either WT or mutant Kv1.2 for outward currents assessment under lipid antigen stimulation. This way, we will be able to provide further evidence that Pyk2-Kv1.2 axis is essential for CD1d-mediated 5-HT release. In addition, while our work demonstrates lipid antigens promote 5-HT release, further investigation is required to validate such iNKT-EC cell crosstalk and signaling cascade in human system. Finally, besides the current study's focus on EC cells of 5-HT release, a potential role of CD1d signaling in other intestinal enteroendocrine cell responses to lipid antigens of hormones release need to be addressed in future work.

STAR Methods

Resource availability

Lead contact—Further information and requests for resources and reagents should be directed to and will be fulfilled by the Lead Contact, Chuan Wu (chuan.wu@nih.gov).

Materials availability—This study did not generate any new unique reagents.

Data and code availability—All data are available in the main text or the supplemental information. This study did not generate any original dataset or code. Any additional information required to reanalyze the data reported in this paper is available from the lead contact upon request.

Experimental model and subject details

Mice

C57BL/6J (WT), *Cd1d*$^{-/-}$, *Traj18*$^{-/-}$, *Va14* Tg, *Cd11c*^{cre}, *Rorc*^{cre}, and *Vil1*^{cre} mice were purchased from Jackson Laboratory; *Pirt*^{GCaMP3} mice were from Dr. Xinzhong Dong; *Tph1*^{flox} mice were from Dr. Gerard Karsenty; *Tph1*^{CFP} mice were from Dr. Andrew B. Leiter; *Cd1d1*^{flox} mice were from MMRRC; *Chga*$^{cre ER}$mice were from EMMA.

Mouse lines were interbred in our facilities to obtain the final strains described in the text. Mice were maintained at the National Cancer Institute facilities under specific pathogenfree conditions. Mice were fed a standard chow diet and used at 7–12 weeks of age for most experiments. All experiments were carried out in accordance with guidelines prescribed by the Institutional Animal Care and Use Committee at the National Cancer Institute. For *Chga*$^{cre ER}$*Cd1d1*$^{fl/fl}$ mice, 1mg Tamoxifen was i.p. injected daily for 5 days before the experiments.

Germ free mice monocolonized with *B. fragilis* strain NCTC 9343 (BFWT) and its mutant strain BFΔSPT were maintained in vinyl isolators in the animal facility as described previously,[20] in accordance with guidelines prescribed by the Institutional Animal Care and Use Committee at Brigham and Women's Hospital.

Oxazolone induced colitis

The mice were presensitized by epicutaneous application of 3% oxazolone (4-ethoxymethylene-2-phenyl-2-oxazolin-5-one; Sigma-Aldrich) in a mixture of 100 μl acetone and olive oil (4:1). 5 days later, the animals were challenged intrarectally (through a 3.5F catheter) with 100 μl 1% oxazolone in 50% ethanol. The control mice will undergo the same procedures but will be administrated with 50% ethanol. The tissues were harvest after challenging at indicated time.

Bead expulsion assay

For colonic propulsion measurement, mice were deprived of the food with access to water overnight for 12hrs on day 0. Before the experiment, the mouse was performed with anesthesia (2.5% Isoflurane), a 2mm diameter glass bead was inserted into the rectum in

the depth of 2cm from the anus with an oil-polished glass rod. Then the mouse was put back into the cage, and the time of the bead expulsion was recorded. The distal colonic transit time was determined by monitoring the time required for the expulsion of the glass bead. Control and experimental groups were age and sex matched. For lipid peptide administration, 200ng α-GalCer (Avanti Polar Lipids) was administered by i.p. injections prior to the assay. For lipid inhibition, GSL-Bf717 was purified as described previously.[20] 1μg GSL-Bf717 was pre-mixed with α-GalCer and i.p injected into the mice before bead expulsion assay.

Carmine red assay

The mice were orally gavaged with 200μL sterilized 6% (w/v) solution of carmine red (Sigma-Aldrich) in 0.5% methylcellulose (Sigma-Aldrich). Fecal output was monitored every 30 min. The time from gavage to appearance of bright red dye was recorded as the whole gut transit time.

CMMC (colonic migrating motor complex) recording

CMMC recording was performed according to previously described.[84] Briefly, the entire mouse colon was removed and transferred to a dish containing warm (35 ± 1°C) Krebs solution: 120mM NaCl, 6mM KCl, 14.4mM $NaHCO_3$, 1.2mM $MgCl_2$, 1.35mM NaH_2PO_4, 12mM glucose, 2.5mM $CaCl_2$ (pH 7.4) bubbled with 95%O_2/5%CO_2. The contraction of circular muscle during each CMMC was recorded using independent isometric force transducers (AD instruments) connected via fine suture thread to hooks that pierced the muscle wall at the proximal, middle and distal region of the colon. Each transducer was connected to an input channel of the bridge amplifier (AD instruments). Data were acquired using the PowerLab data acquisition system operated by LabChart software (AD instruments). For the treatment of 5HT3 receptor antagonist, 5μM Ondansetron (Tocris) was injected into the lumen. For lipid peptide administration, 5μM α-GalCer (Avanti Polar Lipids) was injected into the lumen.

GCaMP fluorescence imaging

The colon was removed and cut open along the mesenteric border from *Pirt*^{GCaMP3} mice. The tissue was pinned flat with mucosal side uppermost to the bottom of a 35mm dish coated with Sylgard-184 (Dow Corning Corp., Midland, MI, USA). Tissue was bathed in Krebs solution. The epithelium layer was removed under a dissecting microscope when indicated. The time-lapse movies of whole mount calcium imaging data were acquired with NIS-elements software using an inverted confocal microscope (Nikon). Data were processed and analyzed using ImageJ software (NIH).[85]

Serotonin quantification

The serum samples or the cell supernatant were harvested. The measurements were performed using Serotonin ELISA Kit (Enzo Life Sciences) according to the manufacturers' protocols.

Tail bleeding assay

The mice were anesthetized with a mixture of ketamine, xylazine and acepromazine. and placed in prone position. A distal 10mm segment of the tail was amputated with a scalpel. The tail was immediately immersed in a 50mL Falcon tube containing isotonic saline prewarmed in a water bath to 37°C. Each animal was monitored for 20min even if bleeding ceased, in order to detect any re-bleeding. Bleeding time was determined using a stop clock. If bleeding on/off cycles occurred, the sum of bleeding times within the 20min period was used. The experiment was terminated at the end of 20min to avoid lethality during the experiment.

Platelet analysis

The platelets were purified from mouse plasma and resuspended with Tyrode's Buffer (134mM NaCl, 0.34mM Na_2HPO_4, 3mM KCl, 12mM $NaHCO_3$, 20mM Hepes pH 7.0, 5mM glucose, 0.35% bovine serum albumin). For flow cytometry analysis, the antibodies anti-CD42b, anti-CD62P and Jon/A (anti-activated CD41/CD61) (Emfret), or anti-Cd1d (Biolegend) were added. For platelet activation, 0.05U/ml thrombin (Sigma) was added together with the antibodies and incubated at room temperature for 15mins. PBS was added to stop the reaction and the platelets were analyzed by FACS within 30mins. All flow cytometry data were acquired on a BD X-20 cell analyzer and analyzed with FlowJo software.

Intestinal organoids generation

Tph1^{CFP} or *Cd1d*$^{-/-}$ *Tph1*^{CFP} mice aged 6–10 weeks were used to generate intestinal organoids, as previously reported.[86] Briefly, the small intestine was isolated and washed with cold PBS and crypts were isolated following dissociation in EDTA. Isolated crypts were suspended in Matrigel. Following polymerization, IntestiCult™ Organoid Growth Medium (Stemcell) was added and refreshed every 3–4days. Organoids were maintained at 37°C, 5% CO2 and propagated weekly.

For lentivirus transduction, mouse Cd1d1 and its intracellular domain truncation were cloned from cDNA clone (Sino biological) into pLV-IRES-mCherry, and transfected into HEK293T cells together with pMD2.g and psPAX2 using lipofectamine 3000 (Invitrogen). The supernatant was harvested 72hrs post transfection and concentrated by ultra-centrifuge. The organoids were dissociated into single cells with TrypLE (Gibco) and mixed with virus in culture for 6hrs at 37°C. Then the cells were collected and re-suspended in Matrigel for culture. The fluorescence was checked after 48hrs.

iNKT cell culture

iNKT cells were purified from the splenocytes of *Va14* Tg mice with PBS-57-loaded mCD1d tetramer (NIH Tetramer Core Facility) and anti-TCRβ by BD Aria sorter, and cultured with mouse T activator anti-CD3/CD28 magnetic beads (Gibco) in a 1:1 ratio plus 20U/mL IL-2 (PeproTech) and 10 ng/mL IL-7 (PeproTech) in complete RPMI. The cells were split in 1:2 when 80–90% confluence for up to 2 weeks.

Biosensor cell culture

$5HT_3R$ were amplified from mouse brain cDNA and cloned into pcDAN3.1-IRESmCherry. The plasmid was transfected into HEK293T cells with lipofectamine 3000 (Invitrogen) 36hrs before imaging.

Calcium imaging

Tph1^{CFP} organoids were dissociated into single cells with TrypLE (Gibco) and cultured in DMEM containing 5% Heat Inactivated FBS, 1% Pen-step, 1% L-Glutamine, and 10 μM Y-27632. Cells were plated on coverslips coated with 5% w/v Matrigel. Cells were maintained in standard culture conditions for 24–48hours. The *Cd1d*$^{-/-}$ *Tph1*^{CFP} cells were labeled with CellTrace™ Far Red (Thermo Fisher) before the culture.

Before imaging, cells were loaded with 4μM Fura-2 AM (Invitrogen) in culture medium at 37°C for 45 min. Cells were then washed with calcium imaging buffer (135mM NaCl, 5mM KCl, 2mM $CaCl_2$, 0.5mM $MgCl_2$, 0.5mM $MgSO_4$, 0.44mM KH_2PO_4, 0.34mM Na_2HPO_4, 10mM HEPES, 10mM glucose, 30mM sucrose, pH 7.45) and analyzed 30min later.

After the coverslip with EC cells were put under the microscope, the iNKT cells or biosensor cells were added into the imaging chamber. The single cell of iNKT or mCherry$^+$ biosensor cells was patched and brought in contact with one CFP$^+$ EC cell.

Fluorescence at 340 nm and 380 nm excitation wavelengths (F340, F380) was recorded using an inverted Nikon Ti-S microscope with NIS-Elements imaging software (Nikon Instruments). The ratio of fluorescence intensities (F340/F380) was used to reflect $[Ca^{2+}]_i$ values. The threshold of activation was defined as three standard deviations above the average. 5μM α-GalCer, 200μM GSL-Bf717, 10μM PF-431396, 100μM KCl and 10μM mCPBG were added during the recording as indicated.

Electrophysiology

Patch-clamp recordings of EC cells were made using a Multiclamp 700B amplifier (Axon Instruments), Digidata 1440A digitizer (Axon Instruments), and pClamp 10.7 software (Axon Instruments). Isolated EC cells from organoids were identified by CFP expression and electrophysiological recordings were made using pipettes pulled from 1.5mm O.D x 1.1mm I.D borosilicate glass capillaries (Sutter Instruments) with resistance ranging between 5–7 MΩ. Recordings were performed at room temperature using extracellular solution containing 140mM NaCl, 5mM KCl, 10mM HEPES, 10mM glucose, 1mM $MgCl_2$, 2mM $CaCl_2$, pH 7.4. The internal solution contained 140mM K-gluconate, 5mM NaCl, 1mM MgCl2, 0.02mM K-EGTA, 10mM HEPES, 10mM sucrose, pH 7.2. After obtaining whole-cell configuration, EC cells were held at – 90mV and currents elicited from 500ms voltage steps ranging between –100 to 100mV at 10mV increments were recorded. During recordings, EC cells were positioned under a three-barreled, square glass tubing and perfusion of solutions were made using a VCS-8, computer-controlled valve system (Warner Instruments, USA) and a VCS-77CSP8 fast perfusion stepper (Warner Instruments, USA). For K^+ recordings, the current-voltage relationship for each EC cell was obtained first under constant perfusion of control wash solution containing external solution only, followed by

50nM TsTx-Kα (Alomone labs), and 10mM tetraethylammonium (TEA, Sigma) diluted in external solution prior to recording. One iNKT cell was first patched and brought in contact with the EC cell, and the current-voltage relationship for each EC cell was obtained similarly, first under constant perfusion of control wash solution containing external solution only, then followed by 5μM α-GalCer. During Pyk2 inhibition, both wash and α-GalCer solutions contained 10μM PF 431396. Data were sampled at 10kHz and filtered at 2kHz. Series resistance (Rs) was monitored during recording and not compensated. Recordings that exhibited greater than 25% variability in Rs were discarded.

CD1d crosslinking

BON-1 cell line was obtained from Dr. Mark R. Hellmich from The University of Texas Medical Branch. The cells were cultured in DMEM/F12 with 10% FBS. The cells were crosslinked with the addition of 10μg/ml anti-CD1d antibody (51.1, eBioscience) for 1hr and followed by washing and addition of 10μg/ml secondary rat anti-mouse IgG2a antibody for indicated time. 10μM PF-431396 were added together with the antibodies as indicated.

Tph1^{CFP} organoids were broken from the Matrigel and culture in the growth media. The crosslinking was performed by adding 10μg/ml anti-Cd1d antibody (1B1, Thermo Fisher) for 1 hr. The organoids were then washed and added with 10μg/ml secondary donkey antirat IgG antibody for 10 mins.

Intestinal histology and immunofluorescence staining

Mouse colon was fixed in 10% neutral formalin and stored in 70% ethanol. Intestinal samples were then paraffin-embedded and cut into 10μm longitudinal sections by Histoserv Inc. (Germantown, MD). For immunofluorescence staining, slides were deparaffinized by xylene and antigen retrieval was conducted for 20min in a 95°C-water bath in 10 mM sodium citrate, pH 6.0 followed by a 15min incubation at room temperature. Slides were washed, blocked in 5% bovine serum albumin, and stained with the indicated primary antibodies and secondary antibodies conjugated to Alexa fluor 488, 633 or 594 (Thermo Fisher). Slides were mounted in Fluoromount-G (Thermo Fisher), and 3–15 images were taken per slide at 20X or 40X magnification along transections of the intestinal crypts for each biological replicate (Zeiss). For 5-HT and ChgA staining, numbers of positively stained puncta were scored blindly, normalized to total area of intestinal mucosa using ImageJ software (NIH), and then averaged across biological replicates.

For mCD1d tetramer staining, the colon tissues were freshly embedded in O.C.T. compound and the frozen section was incubated in PBS containing 1:10 dilution of PE labeled PBS-57 loaded CD1d tetramer (NIH Tetramer Core Facility) at 4°C overnight. Then the tissues were washed three times with PBS, fixed with 4% paraformaldehyde (PFA) for 1 hr.

Flow cytometry

Intestine tissues were isolated and were incubated at 37 °C for 20 min in PBS media containing 2% FBS, 5mM EDTA and 1mM DTT. To isolate intraepithelial lymphocytes, cells derived from the epithelial compartment were purified from percoll centrifuge. For lamina propria lymphocytes, the remaining tissues were cut into smaller pieces and

incubated in RPMI-1640 containing 5% FBS, 1mg/ml collagenase D for 1h at 37 °C under constant horizontal shaking. The digested tissues were filtered through a 40μm strainer and the lymphocytes were harvested for flow cytometry staining. PE-conjugated PBS-57loaded mCD1d tetramer (NIH Tetramer Core Facility) and APC-anti-TCRβ were added to identify iNKT cells. All flow cytometry data were acquired on a BD LSRFortessa™ X-20 cell analyzer and analyzed with FlowJo software.

Western blot

The cells were lysed in whole cell extract buffer (50mM Tris-HCl, pH 7.5, 150mM NaCl, 1% NP-40, 0.2mM EDTA, 10mM Na_3VO_4, 10% glycerol, protease inhibitors). Proteins were separated by gel electrophoresis using 4–12% Bis-Tris gels (Genscript) followed by transfer to nitrocellulose membrane. Membranes were incubated with 5% milk in TBST (150mM NaCl, 20mM Tris-HCl, pH 7.5, 0.1% (v/v) Tween-20) for 60min and washed once with TBST. Proteins of interest were detected by incubating membranes over night at 4°C in blocking buffer with primary antibodies, washing with TBST three times for 10min and incubating with horseradish peroxidase-conjugated anti-rabbit or anti-mouse antibody. Blotting signaling was detected with SuperSignal™ West Pico PLUS Chemiluminescent Substrate (Thermo Fisher).

Immunoprecipitation

Cell lysates were incubated with 5μg anti-pTyr (Cell Signaling)) overnight at 4°C and then added with Protein A/G Dynabeads (Invitrogen). Beads were washed extensively, and proteins were eluted with loading buffer. The presence of proteins in immunocomplexes was determined by immunoblot analysis.

Proximity-ligation assay.

The proximity-ligation assay was performed using a Duolink in situ detection kit (Sigma) with a PLA probe anti-rabbit Plus and a PLA probe anti-mouse Minus. The colon section was treated with xylene and antigen retrieval as described above. The procedures for blocking and administrating the primary antibodies, proximity-ligation assay probes, hybridization, ligation, amplification, detection, and mounting followed the manufacturer's recommended protocol. The slides were observed using a confocal microscope.

Quantitative RT-PCR

For gene expression detection, total RNA was isolated from whole cells using the Qiagen miniRNA extraction kit following the manufacturer's instructions. RNA was quantified and complementary DNA was reverse-transcribed using the iScript kit (Biorad) following the manufacturer's instructions. The cDNA samples were used at 20ng/well in a 384 well plate and run in triplicate. PCR reactions were set up using TaqMan Universal PCR Master Mix (Applied Biosystems) on an ABI Prism 7500 Sequence Detection System. Quantification of relative mRNA expression was normalized to the expression of β-Actin.

Statistical analysis

Data were represented was mean ± SEM. Statistical analyses were performed with Graphpad Prism 5.0 (Graph Pad software, La Jolla, CA, USA) using an unpaired two-tailed Student's t-test for two groups. ANOVA was used for more than two groups followed by the Tukey post hoc test. Statistical significance was defined as $P < 0.05$.

Supplementary Material

Refer to Web version on PubMed Central for supplementary material.

Acknowledgements

We thank Dr. Xinzhong Dong (Johns Hopkins School of Medicine) for the *Pirt*^{GCaMP3} mice; Dr. Gerard Karsenty (Columbia University) for the *Tph1*^{flox} mice; Dr. Andrew B. Leiter (University of Massachusetts Medical School) for the *Tph1*^{CFP} mice. Dr. Mark Hellmich (UTMB Health) for BON-1 cell line. We thank Joelle Mornini, NIH Library, for manuscript editing assistance. We thank Dr. Wei Li (National Eye Institute), Dr. Yuefeng Huang (Columbia University) and Dr. Ye Zheng (Salk Institute) for critical review of the manuscript.

This work was supported by the Intramural Research Program of the National Cancer Institute, Center for Cancer Research, National Institutes of Health.

Reference:

1. Furness JB, Rivera LR, Cho HJ, Bravo DM, and Callaghan B (2013). The gut as a sensory organ. Nat Rev Gastroenterol Hepatol 10, 729–740. 10.1038/nrgastro.2013.180. [PubMed: 24061204]
2. Hoffman JM, and Margolis KG (2020). Building community in the gut: a role for mucosal serotonin. Nat Rev Gastroenterol Hepatol 17, 6–8. 10.1038/s41575-019-0227-6. [PubMed: 31624372]
3. Gershon MD, and Tack J (2007). The serotonin signaling system: from basic understanding to drug development for functional GI disorders. Gastroenterology 132, 397–414. 10.1053/j.gastro.2006.11.002. [PubMed: 17241888]
4. Brown DR (1996). Mucosal protection through active intestinal secretion: neural and paracrine modulation by 5-hydroxytryptamine. Behav Brain Res 73, 193–197. 10.1016/0166-4328(96)00095-2. [PubMed: 8788501]
5. Heredia DJ, Dickson EJ, Bayguinov PO, Hennig GW, and Smith TK (2009). Localized release of serotonin (5-hydroxytryptamine) by a fecal pellet regulates migrating motor complexes in murine colon. Gastroenterology 136, 1328–1338. 10.1053/j.gastro.2008.12.010. [PubMed: 19138686]
6. Jin JG, Foxx-Orenstein AE, and Grider JR (1999). Propulsion in guinea pig colon induced by 5-hydroxytryptamine (HT) via 5-HT4 and 5-HT3 receptors. J Pharmacol Exp Ther 288, 93–97. [PubMed: 9862758]
7. Launay JM, Herve P, Peoc'h K, Tournois C, Callebert J, Nebigil CG, Etienne N, Drouet L, Humbert M, Simonneau G, and Maroteaux L (2002). Function of the serotonin 5-hydroxytryptamine 2B receptor in pulmonary hypertension. Nature medicine 8, 1129–1135. 10.1038/nm764.
8. Yadav VK, Balaji S, Suresh PS, Liu XS, Lu X, Li Z, Guo XE, Mann JJ, Balapure AK, Gershon MD, et al. (2010). Pharmacological inhibition of gut-derived serotonin synthesis is a potential bone anabolic treatment for osteoporosis. Nature medicine 16, 308–312. 10.1038/nm.2098.
9. Crane JD, Palanivel R, Mottillo EP, Bujak AL, Wang H, Ford RJ, Collins A, Blumer RM, Fullerton MD, Yabut JM, et al. (2015). Inhibiting peripheral serotonin synthesis reduces obesity and metabolic dysfunction by promoting brown adipose tissue thermogenesis. Nature medicine 21, 166–172. 10.1038/nm.3766.
10. Baganz NL, and Blakely RD (2013). A dialogue between the immune system and brain, spoken in the language of serotonin. ACS Chem Neurosci 4, 48–63. 10.1021/cn300186b. [PubMed: 23336044]

11. Mercado CP, Quintero MV, Li Y, Singh P, Byrd AK, Talabnin K, Ishihara M, Azadi P, Rusch NJ, Kuberan B, et al. (2013). A serotonin-induced N-glycan switch regulates platelet aggregation. Sci Rep 3, 2795. 10.1038/srep02795. [PubMed: 24077408]
12. Motomura Y, Ghia JE, Wang H, Akiho H, El-Sharkawy RT, Collins M, Wan Y, McLaughlin JT, and Khan WI (2008). Enterochromaffin cell and 5-hydroxytryptamine responses to the same infectious agent differ in Th1 and Th2 dominant environments. Gut 57, 475–481. 10.1136/gut.2007.129296. [PubMed: 18198200]
13. Wang H, Steeds J, Motomura Y, Deng Y, Verma-Gandhu M, El-Sharkawy RT, McLaughlin JT, Grencis RK, and Khan WI (2007). CD4+ T cell-mediated immunological control of enterochromaffin cell hyperplasia and 5-hydroxytryptamine production in enteric infection. Gut 56, 949–957. 10.1136/gut.2006.103226. [PubMed: 17303597]
14. Manocha M, Shajib MS, Rahman MM, Wang H, Rengasamy P, Bogunovic M, Jordana M, Mayer L, and Khan WI (2013). IL-13-mediated immunological control of enterochromaffin cell hyperplasia and serotonin production in the gut. Mucosal immunology 6, 146–155. 10.1038/mi.2012.58. [PubMed: 22763407]
15. Chen Z, Luo J, Li J, Kim G, Stewart A, Urban JF Jr., Huang Y, Chen S, Wu LG, Chesler A, et al. (2021). Interleukin-33 Promotes Serotonin Release from Enterochromaffin Cells for Intestinal Homeostasis. Immunity 54, 151–163 e156. 10.1016/j.immuni.2020.10.014. [PubMed: 33220232]
16. Kronenberg M (2005). Toward an understanding of NKT cell biology: progress and paradoxes. Annual review of immunology 23, 877–900. 10.1146/annurev.immunol.23.021704.115742.
17. Benlagha K, Kyin T, Beavis A, Teyton L, and Bendelac A (2002). A thymic precursor to the NK T cell lineage. Science 296, 553–555. 10.1126/science.1069017. [PubMed: 11968185]
18. Bai L, Constantinides MG, Thomas SY, Reboulet R, Meng F, Koentgen F, Teyton L, Savage PB, and Bendelac A (2012). Distinct APCs explain the cytokine bias of alpha-galactosylceramide variants in vivo. Journal of immunology 188, 3053–3061. 10.4049/jimmunol.1102414.
19. Hayakawa Y, Takeda K, Yagita H, Van Kaer L, Saiki I, and Okumura K (2001). Differential regulation of Th1 and Th2 functions of NKT cells by CD28 and CD40 costimulatory pathways. Journal of immunology 166, 6012–6018. 10.4049/jimmunol.166.10.6012.
20. An D, Oh SF, Olszak T, Neves JF, Avci FY, Erturk-Hasdemir D, Lu X, Zeissig S, Blumberg RS, and Kasper DL (2014). Sphingolipids from a symbiotic microbe regulate homeostasis of host intestinal natural killer T cells. Cell 156, 123–133. 10.1016/j.cell.2013.11.042. [PubMed: 24439373]
21. Saez de Guinoa J, Jimeno R, Gaya M, Kipling D, Garzon MJ, Dunn-Walters D, Ubeda C, and Barral P (2018). CD1d-mediated lipid presentation by CD11c(+) cells regulates intestinal homeostasis. EMBO J 37. 10.15252/embj.201797537.
22. Nieuwenhuis EE, Matsumoto T, Lindenbergh D, Willemsen R, Kaser A, SimonsOosterhuis Y, Brugman S, Yamaguchi K, Ishikawa H, Aiba Y, et al. (2009). Cd1ddependent regulation of bacterial colonization in the intestine of mice. The Journal of clinical investigation 119, 1241–1250. 10.1172/JCI36509. [PubMed: 19349688]
23. van de Wal Y, Corazza N, Allez M, Mayer LF, Iijima H, Ryan M, Cornwall S, Kaiserlian D, Hershberg R, Koezuka Y, et al. (2003). Delineation of a CD1d-restricted antigen presentation pathway associated with human and mouse intestinal epithelial cells. Gastroenterology 124, 1420–1431. 10.1016/s0016-5085(03)00219-1. [PubMed: 12730881]
24. Perera L, Shao L, Patel A, Evans K, Meresse B, Blumberg R, Geraghty D, Groh V, Spies T, Jabri B, and Mayer L (2007). Expression of nonclassical class I molecules by intestinal epithelial cells. Inflammatory bowel diseases 13, 298–307. 10.1002/ibd.20026. [PubMed: 17238179]
25. Bleicher PA, Balk SP, Hagen SJ, Blumberg RS, Flotte TJ, and Terhorst C (1990). Expression of murine CD1 on gastrointestinal epithelium. Science 250, 679–682. 10.1126/science.1700477. [PubMed: 1700477]
26. Im JS, Arora P, Bricard G, Molano A, Venkataswamy MM, Baine I, Jerud ES, Goldberg MF, Baena A, Yu KO, et al. (2009). Kinetics and cellular site of glycolipid loading control the outcome of natural killer T cell activation. Immunity 30, 888–898. 10.1016/j.immuni.2009.03.022. [PubMed: 19538930]

27. Kawano T, Cui J, Koezuka Y, Toura I, Kaneko Y, Motoki K, Ueno H, Nakagawa R, Sato H, Kondo E, et al. (1997). CD1d-restricted and TCR-mediated activation of valpha14 NKT cells by glycosylceramides. Science 278, 1626–1629. 10.1126/science.278.5343.1626. [PubMed: 9374463]
28. Fuss IJ, Heller F, Boirivant M, Leon F, Yoshida M, Fichtner-Feigl S, Yang Z, Exley M, Kitani A, Blumberg RS, et al. (2004). Nonclassical CD1d-restricted NK T cells that produce IL-13 characterize an atypical Th2 response in ulcerative colitis. The Journal of clinical investigation 113, 1490–1497. 10.1172/JCI19836. [PubMed: 15146247]
29. Fuss IJ, Joshi B, Yang Z, Degheidy H, Fichtner-Feigl S, de Souza H, Rieder F, Scaldaferri F, Schirbel A, Scarpa M, et al. (2014). IL-13Ralpha2-bearing, type II NKT cells reactive to sulfatide self-antigen populate the mucosa of ulcerative colitis. Gut 63, 1728–1736. 10.1136/gutjnl-2013-305671. [PubMed: 24515806]
30. Olszak T, Neves JF, Dowds CM, Baker K, Glickman J, Davidson NO, Lin CS, Jobin C, Brand S, Sotlar K, et al. (2014). Protective mucosal immunity mediated by epithelial CD1d and IL-10. Nature 509, 497–502. 10.1038/nature13150. [PubMed: 24717441]
31. Medzhitov R (2021). The spectrum of inflammatory responses. Science 374, 1070–1075. 10.1126/science.abi5200. [PubMed: 34822279]
32. Heller F, Fuss IJ, Nieuwenhuis EE, Blumberg RS, and Strober W (2002). Oxazolone colitis, a Th2 colitis model resembling ulcerative colitis, is mediated by IL-13producing NK-T cells. Immunity 17, 629–638. 10.1016/s1074-7613(02)00453-3. [PubMed: 12433369]
33. Boirivant M, Fuss IJ, Chu A, and Strober W (1998). Oxazolone colitis: A murine model of T helper cell type 2 colitis treatable with antibodies to interleukin 4. The Journal of experimental medicine 188, 1929–1939. 10.1084/jem.188.10.1929. [PubMed: 9815270]
34. Kiesler P, Fuss IJ, and Strober W (2015). Experimental Models of Inflammatory Bowel Diseases. Cell Mol Gastroenterol Hepatol 1, 154–170. 10.1016/j.jcmgh.2015.01.006. [PubMed: 26000334]
35. Brennan PJ, Brigl M, and Brenner MB (2013). Invariant natural killer T cells: an innate activation scheme linked to diverse effector functions. Nature reviews. Immunology 13, 101–117. 10.1038/nri3369.
36. Sonoda KH, Exley M, Snapper S, Balk SP, and Stein-Streilein J (1999). CD1reactive natural killer T cells are required for development of systemic tolerance through an immune-privileged site. The Journal of experimental medicine 190, 1215–1226. 10.1084/jem.190.9.1215. [PubMed: 10544194]
37. Chandra S, Zhao M, Budelsky A, de Mingo Pulido A, Day J, Fu Z, Siegel L, Smith D, and Kronenberg M (2015). A new mouse strain for the analysis of invariant NKT cell function. Nature immunology 16, 799–800. 10.1038/ni.3203. [PubMed: 26075912]
38. Reilly EC, Wands JR, and Brossay L (2010). Cytokine dependent and independent iNKT cell activation. Cytokine 51, 227–231. 10.1016/j.cyto.2010.04.016. [PubMed: 20554220]
39. Rakhilin N, Barth B, Choi J, Munoz NL, Kulkarni S, Jones JS, Small DM, Cheng YT, Cao Y, LaVinka C, et al. (2016). Simultaneous optical and electrical in vivo analysis of the enteric nervous system. Nat Commun 7, 11800. 10.1038/ncomms11800. [PubMed: 27270085]
40. Chen Z, Luo J, Li J, Kim G, Stewart A, Huang Y, and Wu C (2022). Intestinal IL33 promotes platelet activity for neutrophil recruitment during acute inflammation. Blood 139, 1878–1891. 10.1182/blood.2021013474. [PubMed: 34871362]
41. Walther DJ, Peter JU, Bashammakh S, Hortnagl H, Voits M, Fink H, and Bader M (2003). Synthesis of serotonin by a second tryptophan hydroxylase isoform. Science 299, 76. 10.1126/science.1078197. [PubMed: 12511643]
42. Gershon MD (2013). 5-Hydroxytryptamine (serotonin) in the gastrointestinal tract. Curr Opin Endocrinol Diabetes Obes 20, 14–21. 10.1097/MED.0b013e32835bc703. [PubMed: 23222853]
43. Berger M, Gray JA, and Roth BL (2009). The expanded biology of serotonin. Annu Rev Med 60, 355–366. 10.1146/annurev.med.60.042307.110802. [PubMed: 19630576]
44. McNicol A, and Israels SJ (1999). Platelet dense granules: structure, function and implications for haemostasis. Thromb Res 95, 1–18. 10.1016/s0049-3848(99)00015-8. [PubMed: 10403682]
45. Beikmann BS, Tomlinson ID, Rosenthal SJ, and Andrews AM (2013). Serotonin uptake is largely mediated by platelets versus lymphocytes in peripheral blood cells. ACS Chem Neurosci 4, 161–170. 10.1021/cn300146w. [PubMed: 23336055]

46. Griewank K, Borowski C, Rietdijk S, Wang N, Julien A, Wei DG, Mamchak AA, Terhorst C, and Bendelac A (2007). Homotypic interactions mediated by Slamf1 and Slamf6 receptors control NKT cell lineage development. Immunity 27, 751–762. 10.1016/j.immuni.2007.08.020. [PubMed: 18031695]
47. Cui Y, and Wan Q (2019). NKT Cells in Neurological Diseases. Front Cell Neurosci 13, 245. 10.3389/fncel.2019.00245. [PubMed: 31231193]
48. Liu X, Zhang P, Zhang Y, Wang Z, Xu S, Li Y, Huai W, Zhou Q, Chen X, Chen X, et al. (2019). Glycolipid iGb3 feedback amplifies innate immune responses via CD1d reverse signaling. Cell Res 29, 42–53. 10.1038/s41422-018-0122-7. [PubMed: 30514903]
49. Yuan W, Dasgupta A, and Cresswell P (2006). Herpes simplex virus evades natural killer T cell recognition by suppressing CD1d recycling. Nature immunology 7, 835–842. 10.1038/ni1364. [PubMed: 16845396]
50. Lev S, Moreno H, Martinez R, Canoll P, Peles E, Musacchio JM, Plowman GD, Rudy B, and Schlessinger J (1995). Protein tyrosine kinase PYK2 involved in Ca(2+)induced regulation of ion channel and MAP kinase functions. Nature 376, 737–745. 10.1038/376737a0. [PubMed: 7544443]
51. Dekker LV, and Parker PJ (1994). Protein kinase C--a question of specificity. Trends Biochem Sci 19, 73–77. 10.1016/0968-0004(94)90038-8. [PubMed: 8160269]
52. Werkman TR, Gustafson TA, Rogowski RS, Blaustein MP, and Rogawski MA (1993). Tityustoxin-K alpha, a structurally novel and highly potent K+ channel peptide toxin, interacts with the alpha-dendrotoxin binding site on the cloned Kv1.2 K+ channel. Mol Pharmacol 44, 430–436. [PubMed: 8355670]
53. Sjogren K, Engdahl C, Henning P, Lerner UH, Tremaroli V, Lagerquist MK, Backhed F, and Ohlsson C (2012). The gut microbiota regulates bone mass in mice. J Bone Miner Res 27, 1357–1367. 10.1002/jbmr.1588. [PubMed: 22407806]
54. Wikoff WR, Anfora AT, Liu J, Schultz PG, Lesley SA, Peters EC, and Siuzdak G (2009). Metabolomics analysis reveals large effects of gut microflora on mammalian blood metabolites. Proceedings of the National Academy of Sciences of the United States of America 106, 3698–3703. 10.1073/pnas.0812874106. [PubMed: 19234110]
55. Wieland Brown LC, Penaranda C, Kashyap PC, Williams BB, Clardy J, Kronenberg M, Sonnenburg JL, Comstock LE, Bluestone JA, and Fischbach MA (2013). Production of alpha-galactosylceramide by a prominent member of the human gut microbiota. PLoS biology 11, e1001610. 10.1371/journal.pbio.1001610. [PubMed: 23874157]
56. Bellono NW, Bayrer JR, Leitch DB, Castro J, Zhang C, O'Donnell TA, Brierley SM, Ingraham HA, and Julius D (2017). Enterochromaffin Cells Are Gut Chemosensors that Couple to Sensory Neural Pathways. Cell 170, 185–198 e116. 10.1016/j.cell.2017.05.034. [PubMed: 28648659]
57. Coates MD, Tekin I, Vrana KE, and Mawe GM (2017). Review article: the many potential roles of intestinal serotonin (5-hydroxytryptamine, 5-HT) signalling in inflammatory bowel disease. Aliment Pharmacol Ther 46, 569–580. 10.1111/apt.14226. [PubMed: 28737264]
58. Jorandli JW, Thorsvik S, Skovdahl HK, Kornfeld B, Saeterstad S, Gustafsson BI, Sandvik AK, and van Beelen Granlund A (2020). The serotonin reuptake transporter is reduced in the epithelium of active Crohn's disease and ulcerative colitis. Am J Physiol Gastrointest Liver Physiol 319, G761–G768. 10.1152/ajpgi.00244.2020. [PubMed: 32967429]
59. Stavely R, Fraser S, Sharma S, Rahman AA, Stojanovska V, Sakkal S, Apostolopoulos V, Bertrand P, and Nurgali K (2018). The Onset and Progression of Chronic Colitis Parallels Increased Mucosal Serotonin Release via Enterochromaffin Cell Hyperplasia and Downregulation of the Serotonin Reuptake Transporter. Inflammatory bowel diseases 24, 1021–1034. 10.1093/ibd/izy016. [PubMed: 29668991]
60. Ghia JE, Li N, Wang H, Collins M, Deng Y, El-Sharkawy RT, Cote F, Mallet J, and Khan WI (2009). Serotonin has a key role in pathogenesis of experimental colitis. Gastroenterology 137, 1649–1660. 10.1053/j.gastro.2009.08.041. [PubMed: 19706294]
61. Flamar AL, Klose CSN, Moeller JB, Mahlakoiv T, Bessman NJ, Zhang W, Moriyama S, Stokic-Trtica V, Rankin LC, Putzel GG, et al. (2020). Interleukin-33 Induces the Enzyme Tryptophan Hydroxylase 1 to Promote Inflammatory Group 2 Innate Lymphoid Cell-Mediated Immunity. Immunity 52, 606–619 e606. 10.1016/j.immuni.2020.02.009. [PubMed: 32160524]

62. Leon-Ponte M, Ahern GP, and O'Connell PJ (2007). Serotonin provides an accessory signal to enhance T-cell activation by signaling through the 5-HT7 receptor. Blood 109, 3139–3146. 10.1182/blood-2006-10-052787. [PubMed: 17158224]

63. Mawe GM, and Hoffman JM (2013). Serotonin signalling in the gut--functions, dysfunctions and therapeutic targets. Nat Rev Gastroenterol Hepatol 10, 473–486. 10.1038/nrgastro.2013.105. [PubMed: 23797870]

64. Wirtz S, Popp V, Kindermann M, Gerlach K, Weigmann B, Fichtner-Feigl S, and Neurath MF (2017). Chemically induced mouse models of acute and chronic intestinal inflammation. Nat Protoc 12, 1295–1309. 10.1038/nprot.2017.044. [PubMed: 28569761]

65. Selvanantham T, Lin Q, Guo CX, Surendra A, Fieve S, Escalante NK, Guttman DS, Streutker CJ, Robertson SJ, Philpott DJ, and Mallevaey T (2016). NKT CellDeficient Mice Harbor an Altered Microbiota That Fuels Intestinal Inflammation during Chemically Induced Colitis. Journal of immunology 197, 4464–4472. 10.4049/jimmunol.1601410.

66. Kwon YH, Wang H, Denou E, Ghia JE, Rossi L, Fontes ME, Bernier SP, Shajib MS, Banskota S, Collins SM, et al. (2019). Modulation of Gut Microbiota Composition by Serotonin Signaling Influences Intestinal Immune Response and Susceptibility to Colitis. Cell Mol Gastroenterol Hepatol 7, 709–728. 10.1016/j.jcmgh.2019.01.004. [PubMed: 30716420]

67. Yano JM, Yu K, Donaldson GP, Shastri GG, Ann P, Ma L, Nagler CR, Ismagilov RF, Mazmanian SK, and Hsiao EY (2015). Indigenous bacteria from the gut microbiota regulate host serotonin biosynthesis. Cell 161, 264–276. 10.1016/j.cell.2015.02.047. [PubMed: 25860609]

68. Ayabe T, Satchell DP, Wilson CL, Parks WC, Selsted ME, and Ouellette AJ (2000). Secretion of microbicidal alpha-defensins by intestinal Paneth cells in response to bacteria. Nature immunology 1, 113–118. 10.1038/77783. [PubMed: 11248802]

69. Ayabe T, Wulff H, Darmoul D, Cahalan MD, Chandy KG, and Ouellette AJ (2002). Modulation of mouse Paneth cell alpha-defensin secretion by mIKCa1, a Ca2+- activated, intermediate conductance potassium channel. The Journal of biological chemistry 277, 3793–3800. 10.1074/jbc.M107507200. [PubMed: 11724775]

70. Linan-Rico A, Ochoa-Cortes F, Zuleta-Alarcon A, Alhaj M, Tili E, Enneking J, Harzman A, Grants I, Bergese S, and Christofi FL (2017). UTP - Gated Signaling Pathways of 5-HT Release from BON Cells as a Model of Human Enterochromaffin Cells. Front Pharmacol 8, 429. 10.3389/fphar.2017.00429. [PubMed: 28751862]

71. Nieuwenhuis EE, Neurath MF, Corazza N, Iijima H, Trgovcich J, Wirtz S, Glickman J, Bailey D, Yoshida M, Galle PR, et al. (2002). Disruption of T helper 2immune responses in Epstein-Barr virus-induced gene 3-deficient mice. Proceedings of the National Academy of Sciences of the United States of America 99, 16951–16956. 10.1073/pnas.252648899. [PubMed: 12482940]

72. Page MJ, Poritz LS, Tilberg AF, Zhang WJ, Chorney MJ, and Koltun WA (2000). Cd1d-restricted cellular lysis by peripheral blood lymphocytes: relevance to the inflammatory bowel diseases. The Journal of surgical research 92, 214–221. 10.1006/jsre.2000.5940. [PubMed: 10896824]

73. Zeissig S, Peuker K, Iyer S, Gensollen T, Dougan SK, Olszak T, Kaser A, and Blumberg RS (2017). CD1d-Restricted pathways in hepatocytes control local natural killer T cell homeostasis and hepatic inflammation. Proceedings of the National Academy of Sciences of the United States of America 114, 10449–10454. 10.1073/pnas.1701428114. [PubMed: 28893990]

74. de Pins B, Mendes T, Giralt A, and Girault JA (2021). The Non-receptor Tyrosine Kinase Pyk2 in Brain Function and Neurological and Psychiatric Diseases. Front Synaptic Neurosci 13, 749001. 10.3389/fnsyn.2021.749001. [PubMed: 34690733]

75. Smillie CS, Biton M, Ordovas-Montanes J, Sullivan KM, Burgin G, Graham DB, Herbst RH, Rogel N, Slyper M, Waldman J, et al. (2019). Intra- and Inter-cellular Rewiring of the Human Colon during Ulcerative Colitis. Cell 178, 714–730 e722. 10.1016/j.cell.2019.06.029. [PubMed: 31348891]

76. Ryzhakov G, Almuttaqi H, Corbin AL, Berthold DL, Khoyratty T, Eames HL, Bullers S, Pearson C, Ai Z, Zec K, et al. (2021). Defactinib inhibits PYK2 phosphorylation of IRF5 and reduces intestinal inflammation. Nat Commun 12, 6702. 10.1038/s41467-021-27038-5. [PubMed: 34795257]

77. Spiller R (2007). Recent advances in understanding the role of serotonin in gastrointestinal motility in functional bowel disorders: alterations in 5-HT signalling and metabolism in human disease.

Neurogastroenterol Motil 19 Suppl 2, 25–31. 10.1111/j.1365-2982.2007.00965.x. [PubMed: 17620085]

78. Minderhoud IM, Oldenburg B, Schipper ME, ter Linde JJ, and Samsom M (2007). Serotonin synthesis and uptake in symptomatic patients with Crohn's disease in remission. Clin Gastroenterol Hepatol 5, 714–720. 10.1016/j.cgh.2007.02.013. [PubMed: 17481962]
79. Oh SF, Praveena T, Song H, Yoo JS, Jung DJ, Erturk-Hasdemir D, Hwang YS, Lee CC, Le Nours J, Kim H, et al. (2021). Host immunomodulatory lipids created by symbionts from dietary amino acids. Nature 600, 302–307. 10.1038/s41586-021-04083-0. [PubMed: 34759313]
80. Wingender G, Stepniak D, Krebs P, Lin L, McBride S, Wei B, Braun J, Mazmanian SK, and Kronenberg M (2012). Intestinal microbes affect phenotypes and functions of invariant natural killer T cells in mice. Gastroenterology 143, 418–428. 10.1053/j.gastro.2012.04.017. [PubMed: 22522092]
81. Kim YS, Chu Y, Han L, Li M, Li Z, LaVinka PC, Sun S, Tang Z, Park K, Caterina MJ, et al. (2014). Central terminal sensitization of TRPV1 by descending serotonergic facilitation modulates chronic pain. Neuron 81, 873–887. 10.1016/j.neuron.2013.12.011. [PubMed: 24462040]
82. Yadav VK, Ryu JH, Suda N, Tanaka KF, Gingrich JA, Schutz G, Glorieux FH, Chiang CY, Zajac JD, Insogna KL, et al. (2008). Lrp5 controls bone formation by inhibiting serotonin synthesis in the duodenum. Cell 135, 825–837. 10.1016/j.cell.2008.09.059. [PubMed: 19041748]
83. Li HJ, Johnston B, Aiello D, Caffrey DR, Giel-Moloney M, Rindi G, and Leiter AB (2014). Distinct cellular origins for serotonin-expressing and enterochromaffin-like cells in the gastric corpus. Gastroenterology 146, 754–764 e753. 10.1053/j.gastro.2013.11.048. [PubMed: 24316261]
84. Spencer NJ (2013). Characteristics of colonic migrating motor complexes in neuronal NOS (nNOS) knockout mice. Frontiers in Neuroscience 7. ARTN 184 10.3389/fnins.2013.00184. [PubMed: 24133409]
85. Schneider CA, Rasband WS, and Eliceiri KW (2012). NIH Image to ImageJ: 25 years of image analysis. Nat Methods 9, 671–675. 10.1038/nmeth.2089. [PubMed: 22930834]
86. Sato T, Vries RG, Snippert HJ, van de Wetering M, Barker N, Stange DE, van Es JH, Abo A, Kujala P, Peters PJ, and Clevers H (2009). Single Lgr5 stem cells build crypt-villus structures in vitro without a mesenchymal niche. Nature 459, 262–265. 10.1038/nature07935. [PubMed: 19329995]

Highlights:

1. Lipid-induced gut motility is mediated by 5-HT
2. Enterochromaffin (EC) cell-derived CD1d is critical for 5-HT release
3. Pyk2-Kv1.2 axis is required for gut CD1d-mediated 5-HT release
4. *Bacteroides fragilis* sphingolipids repress intestinal 5-HT secretion

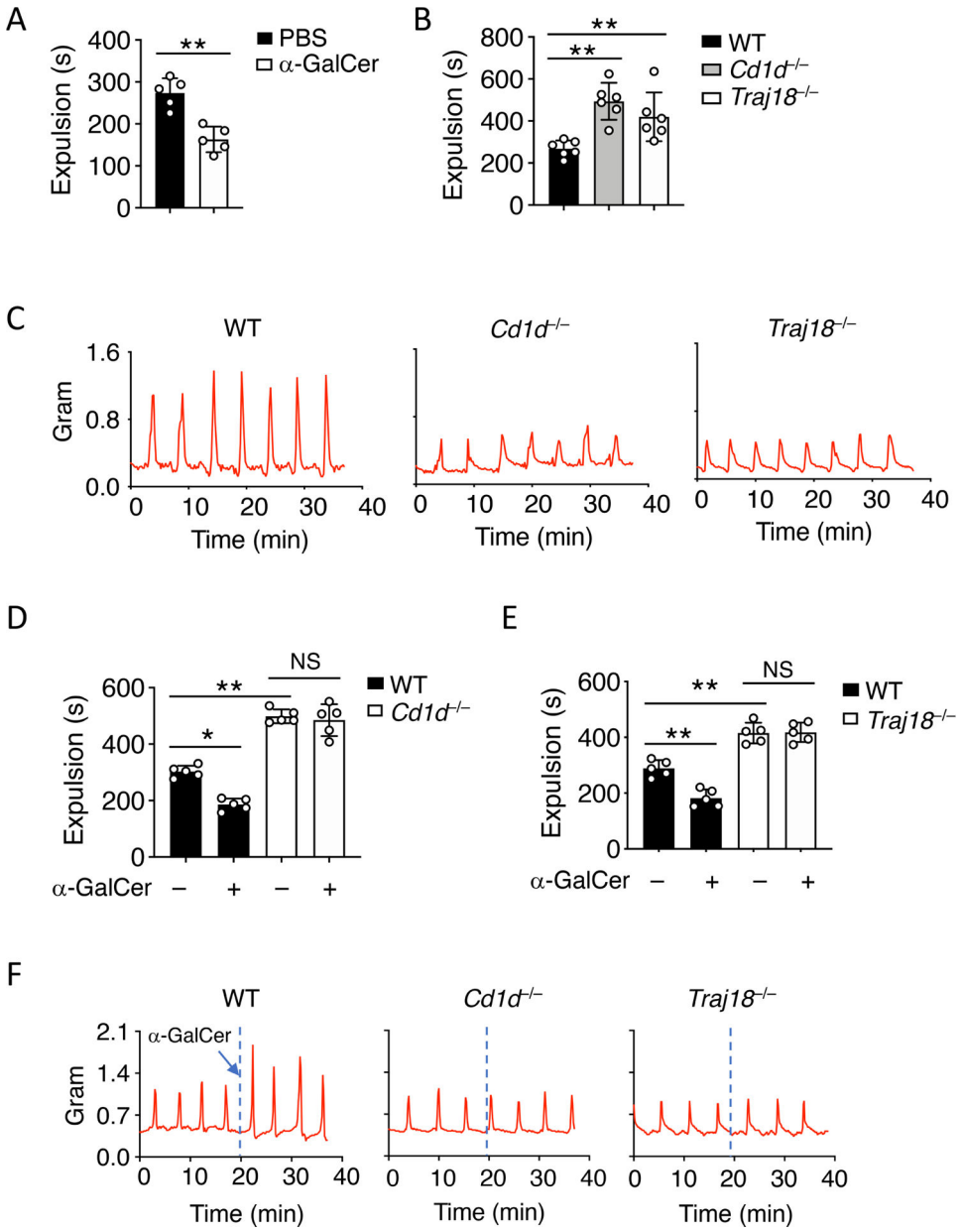

Figure 1. iNKT cell regulates gut motility

(A) WT mice were injected daily with α-GalCer or PBS for 7 days. Colonic transit time was assessed by a bead expulsion assay (n=5 per group, representative data of three experiments).

(B) Colonic transit time was measured by a bead expulsion assay in WT, *Cd1d*$^{-/-}$, and *Traj18*$^{-/-}$ mice under steady state (n=6 per group, representative data of three experiments).

(C) Representative trace of colon contraction in WT, *Cd1d*$^{-/-}$, and *Traj18*$^{-/-}$ mice under steady state (n=3 per group, representative data of three experiments).

(D-E) (D) WT and *Cd1d*$^{-/-}$, (E) WT and *Traj18*$^{-/-}$ mice were injected with PBS or α-GalCer. Colonic transit time was measured by a bead expulsion assay 10 min after injection (n=5 per group, representative data of three experiments).

(F) Representative traces of α-GalCer-induced colon contraction in WT, *Cd1d*$^{-/-}$, and *Traj18*$^{-/-}$ mice (n=3 per group, representative data of three experiments).
NS, not significant; *p<0.05, **p<0.01, (B, One-way ANOVA with Tukey's multiple comparison test; D, E, Two-way ANOVA with Tukey's multiple comparison test; A, Unpaired student's *t*-test; error bars represent SEM). Please also see Figures S1 and S2.

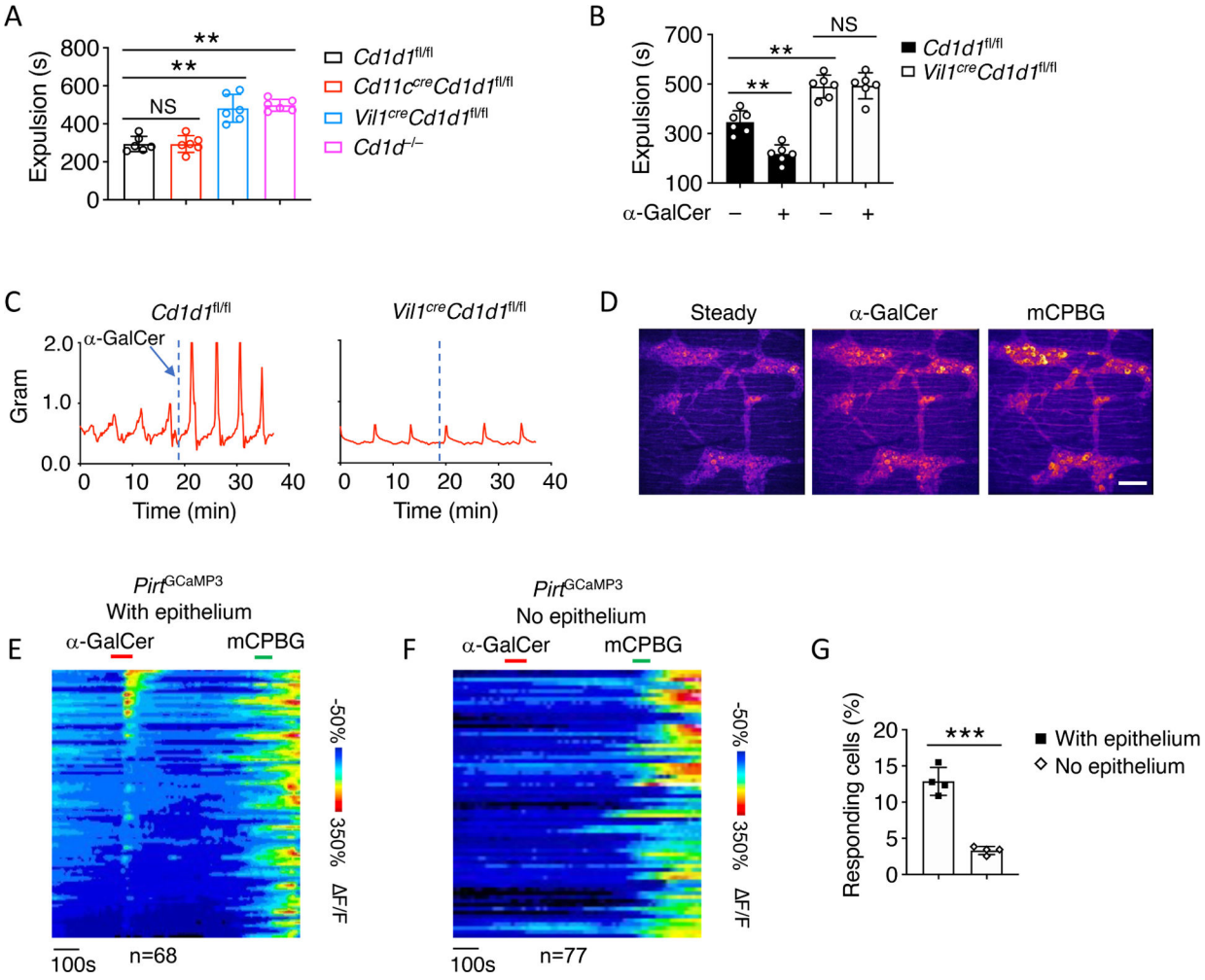

Figure 2. IEC-derived CD1d is required for gut motility

(A) Colonic transit time was assessed by a bead expulsion assay in the indicated mouse strains (n=6 per group, representative data of three experiments).

(B) *Cd1d1*$^{fl/fl}$ and *Vil1*^{cre}*Cd1d1*$^{fl/fl}$ mice were injected with PBS or α-GalCer. Colonic transit time was assessed by a bead expulsion assay 10 min after injection (n=6 per group, representative data of three experiments).

(C) Representative traces of α-GalCer-induced colon contraction in *Cd1d1*$^{fl/fl}$ and *Vil1*^{cre}*Cd1d1*$^{fl/fl}$ mice (n=3 per group, representative data of three experiments).

(D) Representative image of GCaMP3 fluorescence signal of neurons on the myenteric plexus of *Pirt*^{GCaMP3} mice treated with α-GalCer and mCPBG (5-HT$_3$R agonist) (n=3, representative data of three experiments).

(E-G) Time-resolved responses of neurons Time-resolved responses (ΔF/F, color scale) of neurons (one neuron per row) (E) with or (F) without epithelium and (G) pencentage quantification of a-GalCer responding neurons in the myenteric plexus from *Pirt*^{GCaMP3} mice. mCPBG was used as a positive control. Each dot represents percentage of responding neuron in one mouse (n=4 per group, representative data of three experiments).

NS, not significant; **p<0.01, ***p<0.001, (A, One-way ANOVA with Tukey's multiple comparison test; B, Two-way ANOVA with Tukey's multiple comparison test; G, Unpaired student's *t*-test; error bars represent SEM). Please also see Figure S2.

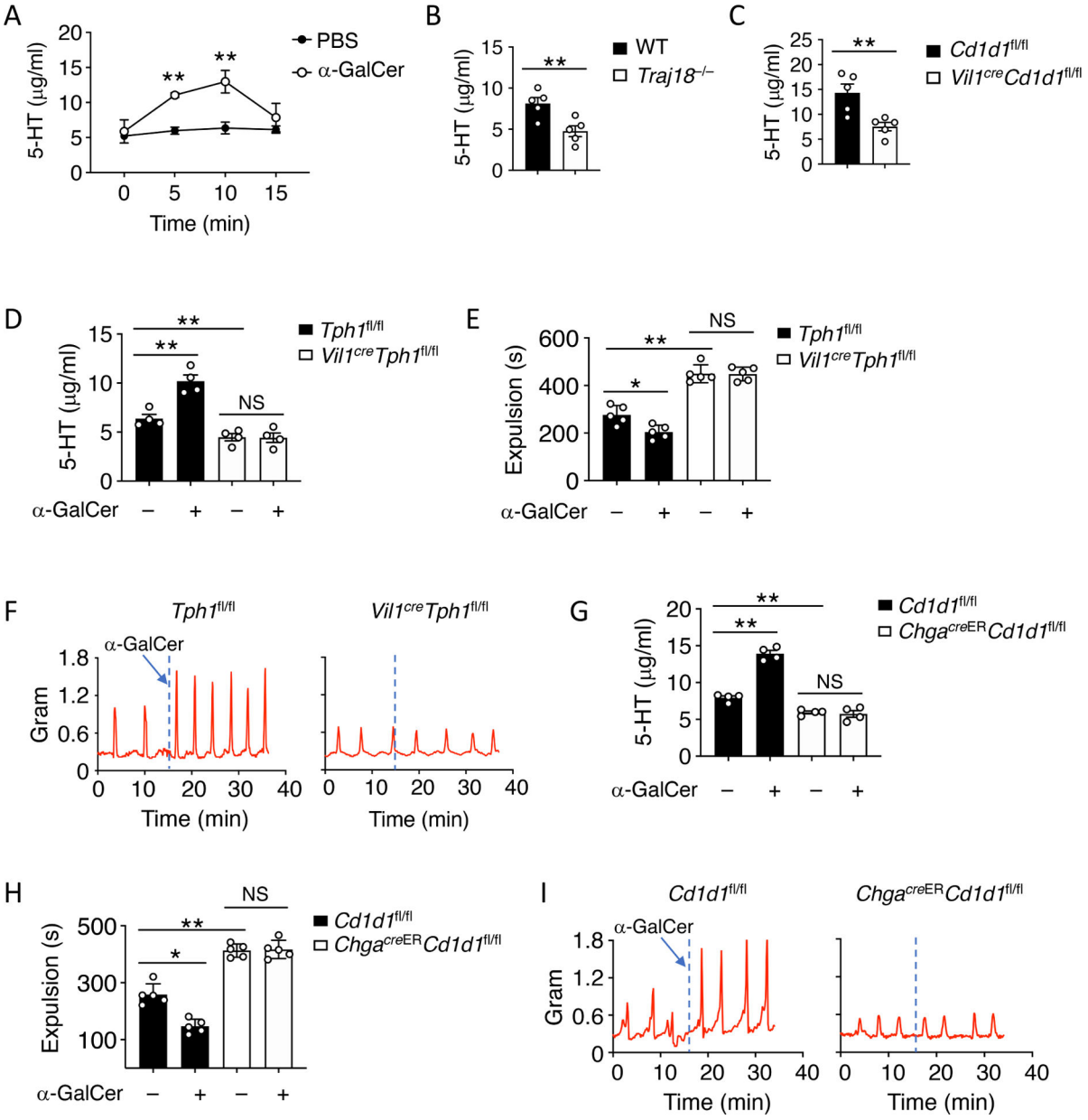

Figure 3. Lipids induce 5-HT secretion from EC cells for gut motility

(A) WT mice were injected with PBS or α-GalCer. Mice serum was collected at the indicated time point, and 5-HT amounts were assessed by ELISA (n=4 per group, representative data of three experiments).

(B-C) 5-HT amounts in (B) WT and *Traj18*$^{-/-}$, (C) *Cd1d1*$^{fl/fl}$ and *Vil1*^{cre}*Cd1d1*$^{fl/fl}$ mice serum under steady state were assessed by ELISA (n=5 per group, pooled data of two experiments).

(D-E) *Tph1*$^{fl/fl}$ and *Vil1*^{cre}*Tph1*$^{fl/fl}$ mice were injected with PBS or α-GalCer. (D) Mice serum was collected 10 min after injection. 5-HT amounts were assessed by ELISA. (E) Colonic transit time was measured by a bead expulsion assay 10 min after treatment (n≥4 per group, representative data of three experiments).

(F) Representative trace of α-GalCer-induced colon contraction in *Tph1*$^{fl/fl}$ and *Vil1*^{cre}*Tph1*$^{fl/fl}$ mice (n=3 per group, representative data of three experiments).
(G-H) *Cd1d1*$^{fl/fl}$ and *Chga*^{creER}*Cd1d1*$^{fl/fl}$ mice were injected with PBS or α-GalCer. (G) Mice serum was collected 10 min after injection. 5-HT amounts were assessed by ELISA.
(H) Colonic transit time was measured by a bead expulsion assay 10 min after treatment (n≥4 per group, representative data of three experiments).
(I) Representative trace of α-GalCer-induced colon contraction in *Cd1d1*$^{fl/fl}$ and *Chga*^{creER}*Cd1d1*$^{fl/fl}$ mice (n=3 per group, representative data of three experiments).
NS: not significant, *p<0.05, **p<0.01, (A, D, E, G, H, Two-way ANOVA with Tukey's multiple comparison test; B, C, Unpaired student's *t*-test; error bars represent SEM). Please also see Figure S3.

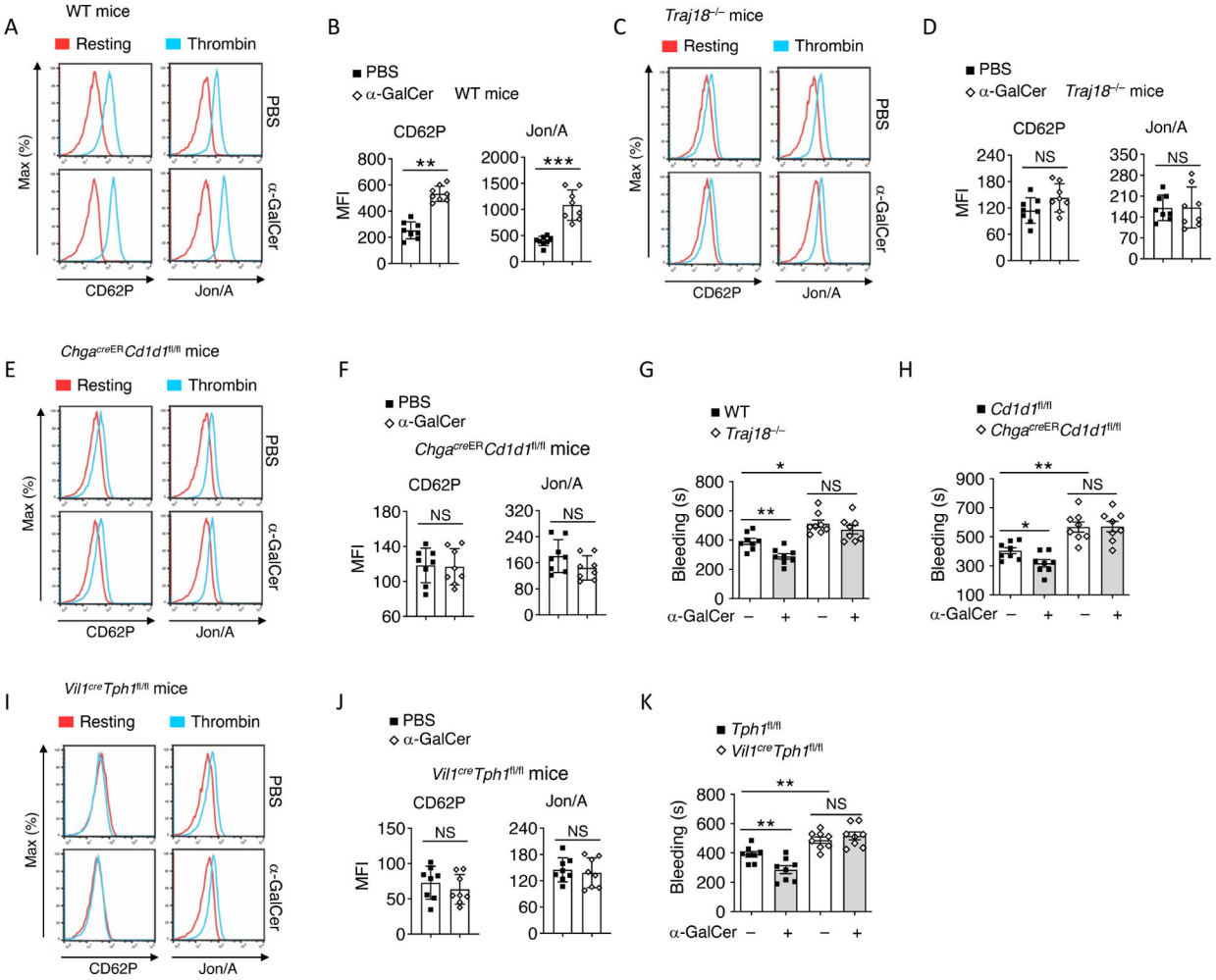

Figure 4. Lipid-mediated 5-HT release rapidly enhances platelet function for hemostasis

(A-F) Indicated mice were injected with PBS or α-GalCer. Platelet activities were assessed by flow cytometry 10 min after injection. Representative histograms of fluorescence intensity and quantification of geometric mean fluorescence intensity of CD62L and JON/A for platelets treated with or without thrombin from (A-B) WT, (C-D) *Traj18*$^{-/-}$, and (E-F) *Chga*^{creER}*Cd1d1*$^{fl/fl}$ mice (n=8 per group, representative data of three experiments).

(G-H) (G) WT and *Traj18*$^{-/-}$, and (H) *Cd1d1*$^{fl/fl}$ and *Chga*^{creER}*Cd1d1*$^{fl/fl}$ mice were injected with PBS or α-GalCer. Time to cessation of bleeding in response to tail injury was assessed 10 min after injection (n=8 per group, representative data of three experiments).

(I-J) *Tph1*$^{fl/fl}$ and *Vil1*^{cre}*Tph1*$^{fl/fl}$ mice were injected with PBS or α-GalCer. Platelet activities were assessed by flow cytometry 10 min after injection. (I) Representative histograms and (J) Quantification of geometric mean fluorescence intensity of CD62L and JON/A for platelets treated with or without thrombin (n=8 per group, representative data of three experiments).

(K) *Tph1*$^{fl/fl}$ and *Vil1*^{cre}*Tph1*$^{fl/fl}$ mice were injected with PBS or α-GalCer. Time to cessation of bleeding in response to tail injury was assessed 10 min after injection (n=8 per group, representative data of three experiments).

NS: not significant, *p<0.05, **p<0.01, ***p<0.001, (G, H, K, Two-way ANOVA with Tukey's multiple comparison test; B, D, F, J, Unpaired student's *t*-test; error bars represent SEM). Please also see Figure S4.

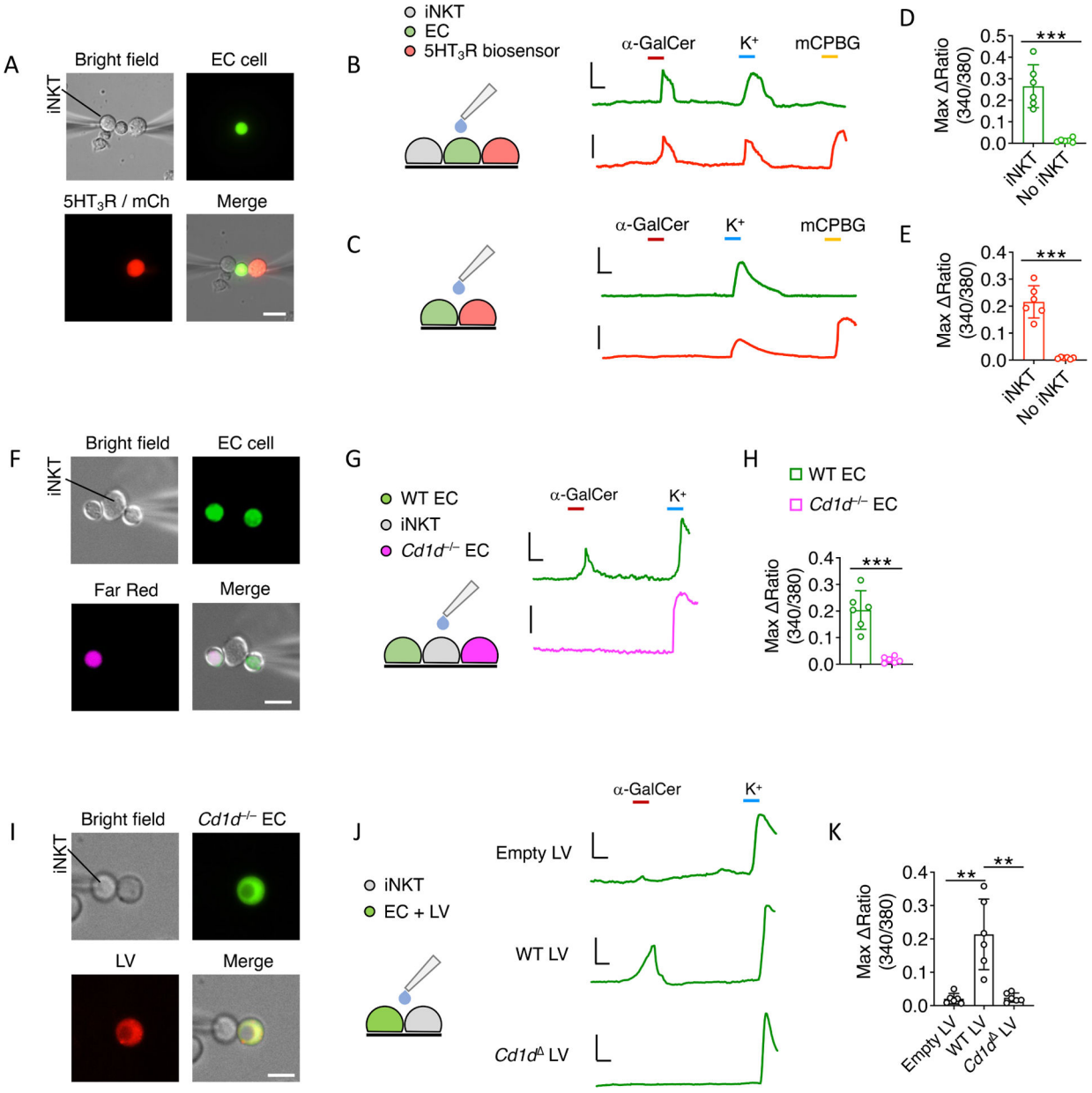

Figure 5. CD1d reverse signal intrinsically modulates 5-HT release from EC cells

(A) Representative image of an EC cell (CFP, green) adjacent to a $5HT_3R$-expressing HEK293 (mCherry, red) cell and an iNKT cell purified from *Va14* Tg mice for simultaneous Ca^{2+} measurements from EC cells and biosensor cells (n=6 per group, representative data of three experiments).

(B-C) (B) Representative trace of Ca^{2+} responses in WT EC cell and biosensor cell under indicated stimulations with or (C) without iNKT cells. Scale bars, 0.3 ΔRatio (340/380), 35 s (n=6 per group, representative data of three experiments).

(D-E) Quantification of α-GalCer responding (D) EC cells and (E) biosensor cells with or without iNKT cells (n=6 per group, representative data of three experiments).

(F) Representative image of a *Tph1*^{CFP} EC cell and a *Cd1d*$^{-/-}$*Tph1*^{CFP} EC cell stained with Far-Red simultaneously adjacent to an iNKT cell for Ca^{2+} measurement (n=6 per group, representative data of three experiments).

(G-H) (G) Representative trace and (H) Quantification of α-GalCer-induced Ca^{2+} responses in WT and *Cd1d*$^{-/-}$ EC cells. Scale bars, 0.2 ΔRatio (340/380), 40 s (n=6 per group, representative data of three experiments).

(I) Representative image of a *Cd1d*$^{-/-}$*Tph1*^{CFP} EC cell lentivirally transduced with indicated genes adjacent to an iNKT cell for Ca^{2+} measurement (n=6 per group, representative data of three experiments).

(J-K) (J) Representative trace and (K) Quantification of α-GalCer-induced Ca^{2+} responses in indicated EC cells. Scale bars, 0.3 ΔRatio (340/380), 30 s (n=6 per group, representative data of three experiments).

**p<0.01, ***p<0.001, (K, One-way ANOVA with Tukey's multiple comparison test; D, E, H, Unpaired student's *t*-test; error bars represent SEM). Please also see Figure S5.

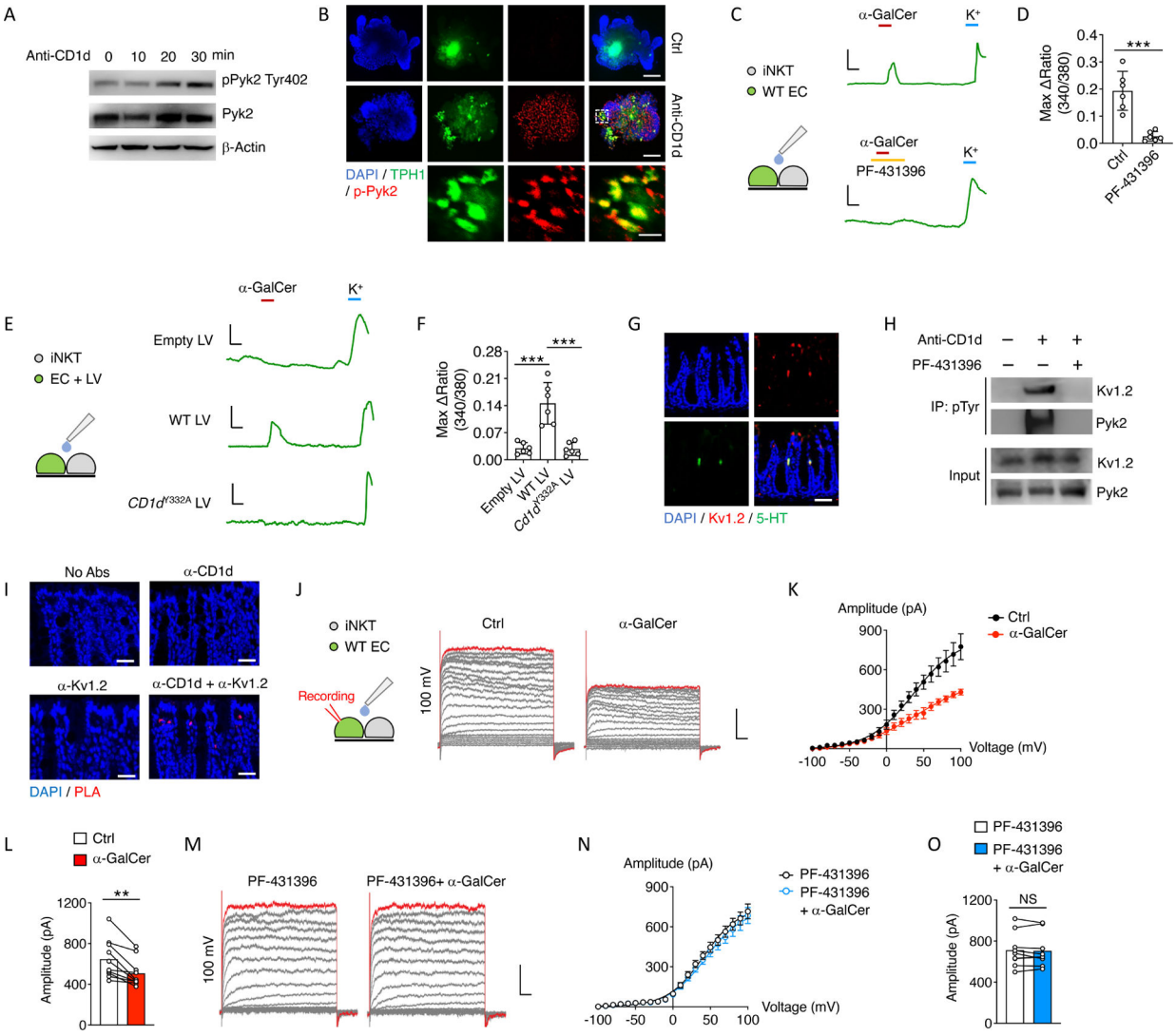

Figure 6. CD1d-mediatd EC cell activation depends on Pyk2-Kv1.2 axis

(A) BON-1 cells were stimulated with crosslinked anti-CD1d. Immunoblot analysis of pPyk2, Pyk2 and α-actin in these cells at the indicated time points (n=3, representative data of three experiments).

(B) *Tph1*^{CFP} EC-enriched intestinal organoids were treated with PBS or crosslinked antiCD1d for 10 min and fixed. Representative immunofluorescence image for TPH1-CFP, pPyk2, and DAPI. Scale bar, 100 μm. Inset scale bar, 20 μm (n=3 per group, representative data of three experiments).

(C-D) (C) Representative trace and (D) Quantification of α-GalCer-induced Ca^{2+} responses in *Tph1*^{CFP} EC cells with or without PF-431396. K^+ was used as a positive control. Scale bars, 0.2 ΔRatio (340/380), 35 s (n=6 per group, representative data of three experiments).

(E-F) *Cd1d*$^{-/-}$*Tph1*^{CFP} EC cell lentivirally transduced with indicated genes adjacent to an iNKT cell for Ca^{2+} measurement. (E) Representative trace and (F) Quantification of α-GalCer induced a Ca^{2+} response in indicated EC cells. Scale bars, 0.2 ΔRatio (340/380), 30 s (n=6 per group, representative data of three experiments).

(G) Representative immunofluorescence staining for 5-HT, Kv1.2 and DAPI in the colonic tissues of WT mice. Scale bar, 10 μm (n=3, representative data of three experiments).
(H) BON-1 cells were stimulated with crosslinked anti-CD1d. Co-immunoprecipitation (IP), with antibody to anti-pTyr of proteins from lysates of BON-1 cells, detected by immunoblot analysis with anti-Kv1.2 or anti-Pyk2 (n=3, representative data of three experiments).
(I) *In situ* proximity-ligation assay (PLA) of colonic tissues from WT mice in the absence of primary antibodies (No Abs) or in the presence of various combinations of anti-CD1d and anti-Kv1.2; punctate staining (red) indicates the CD1d-Kv1.2 interaction. Scale bar, 10 μm (n=3, representative data of three experiments).
(J) Representative K^+ currents in EC cells in the presence or absence of α-GalCer using 500 ms voltage steps ranging from −100 to 100 mV. EC cells were held at −90 mV during voltage steps. Red traces show representative K^+ currents in response to voltage step to 100 mV. Scale bars, 200 pA, 50 ms (n=10, representative data of two experiments).
(K) Current-voltage relationship of the steady-state K^+ currents in EC cells in the presence of wash solution or α-GalCer (n=10, representative data of two experiments).
(L) Steady-state K^+ current in EC cells in response to voltage step to 100 mV in the presence of wash solution or α-GalCer (n=10, pooled data of two experiments).
(M) Representative K^+ currents in EC cells with PF-431396 in the presence or absence of α-GalCer using 500 ms voltage steps ranging from −100 to 100 mV. EC cells were held at −90 mV between voltage steps. Red traces show representative K^+ currents in response to voltage step to 100 mV. Scale bars, 200 pA, 50 ms (n=9, representative data of two experiments).
(N) Current-voltage relationship of the steady-state K^+ currents in EC cells in the presence of PF-431396 with or without α-GalCer (n=9, representative data of two experiments). (O) Steady-state K^+ current in EC cells in response to voltage step to 100 mV in the presence of PF-431396 with or without α-GalCer (n=9, pooled data of two experiments).
NS: not significant, **p<0.01, ***p<0.001, (K, N, Two-way ANOVA with Tukey's multiple comparison test; D, F, Unpaired student's *t*-test; L, O, Paired student's *t*-test, error bars represent SEM). Please also see Figure S6.

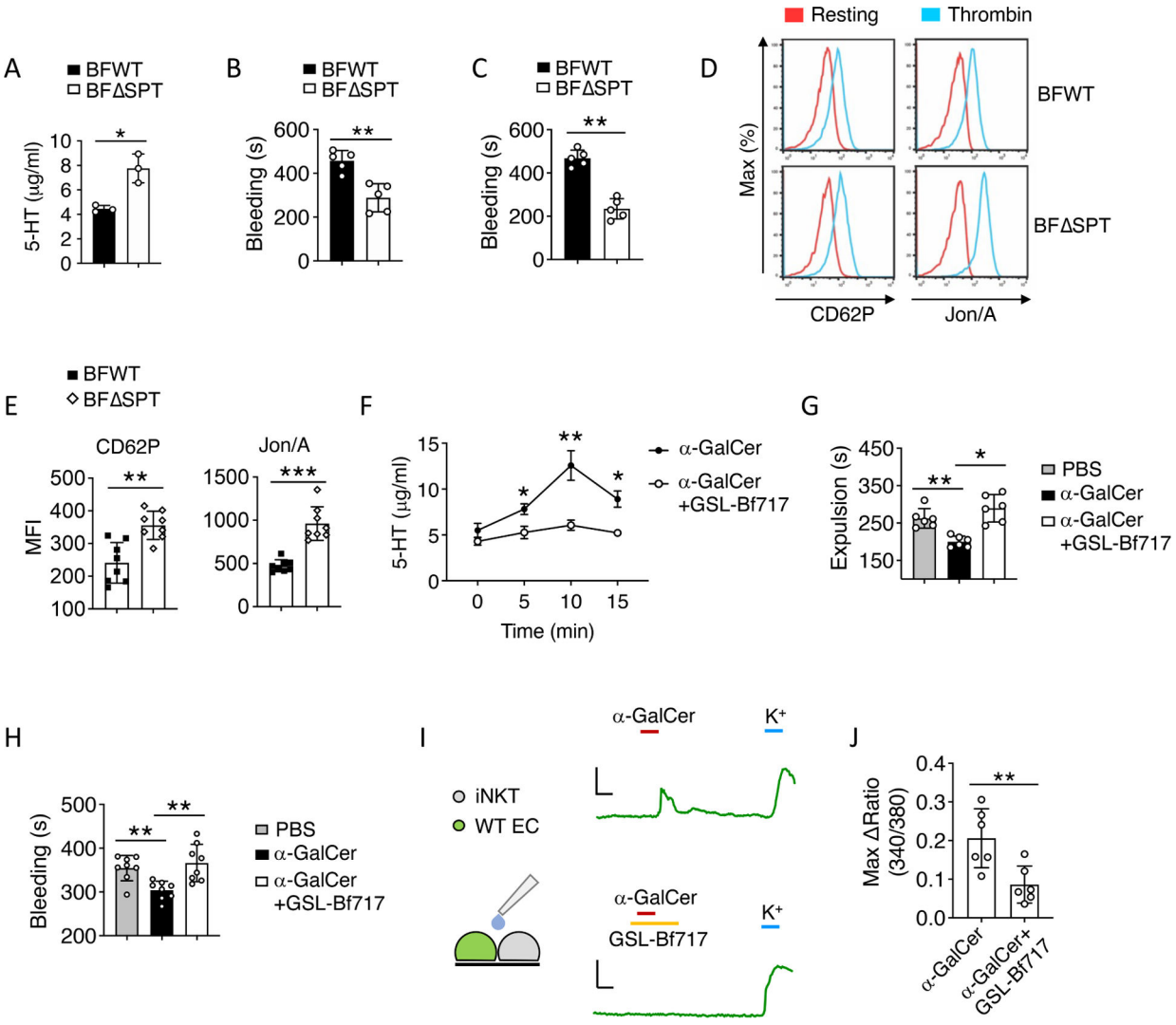

Figure 7. Bacteroides fragilis sphingolipids repress intestinal 5-HT secretion

(A) Relative 5-HT amounts in BFWT and BFΔSPT mice serum under steady state were assessed by ELISA (n=3, representative data of three experiments).

(B) Colonic transit time was assessed by a bead expulsion assay between BFWT and BFΔSPT mice under steady state (n=5, representative data of three experiments).

(C) Time to cessation of bleeding in response to tail injury between BFWT and BFΔSPT mice (n=5, representative data of two experiments).

(D-E) (D) Representative histograms and (E) Quantification of geometric mean fluorescence intensity of CD62P and Jon/A for platelets treated with or without thrombin between BFWT and BFΔSPT mice (n=8, pooled data of two experiments).

(F-H) WT mice were injected with α-GalCer with or without GSL-Bf717. (F) Mice serum was collected at the indicated time point, and relative 5-HT amounts were assessed by ELISA (n=3 per group); (G) Colonic transit time was assessed by a bead expulsion assay10 min after injection (n=6 per group); (H) Time to cessation of bleeding in response to tail injury was assessed 10 min after injection (n=8 per group, representative data of three experiments).

(I-J) (I) Representative trace and (J) Quantification of α-GalCer-induced Ca^{2+} responses in *Tph1*^{CFP} EC cells with or without GSL-Bf717. K^+ was used as a positive control. Scale bars, 0.2 ΔRatio (340/380), 35 s (n=6 per group, representative data of two experiments). *p<0.05, **p<0.01, ***p<0.001, (G, H, One-way ANOVA with Tukey's multiple comparison test; F, Two-way ANOVA with Tukey's multiple comparison test; A-C, E, J, Unpaired student's *t*-test; error bars represent SEM). Please also see Figure S7.

Key resources table

REAGENT or RESOURCE	SOURCE	IDENTIFIER
Antibodies		
DyLight 649 anti-mouse CD42b	Emfret	Cat# M040–3, RRID: AB_2934080
FITC anti-mouse CD62P	Emfret	Cat# M130–1, RRID: AB_2890922
PE anti-mouse CD41/61(Jon/A)	Emfret	Cat# M023–2, RRID: AB_2833084
PE PBS-57-loaded mCD1d tetramer	NIH Tetramer Core Facility	N/A
PE anti-mouse Cd1d	Biolegend	Cat# 123509, RRID: AB_1236547
APC/Fire 750 anti-mouse CD45	Biolegend	Cat# 103154, RRID: AB_2572116
BV421 anti-mouse CD326 (Ep-CAM)	Biolegend	Cat# 118225, RRID: AB_2563983
anti-Human CD1d	Thermo Fisher Scientific	Cat# 14–0016–82, RRID: AB_837139
rat anti-mouse IgG2a	Thermo Fisher Scientific	Cat# RMG2a00, RRID: AB_2556584
anti-mouse Cd1d for crosslinking	Thermo Fisher Scientific	Cat# 14–0011–82, RRID: AB_467036
donkey anti-rat IgG	Thermo Fisher Scientific	Cat# A18747, RRID: AB_2535524
APC anti-TCRβ	Biolegend	Cat# 109211, RRID: AB_313434
PE anti-mouse NK1.1	Thermo Fisher Scientific	Cat# 12–5941–82, RRID: AB_466050
anti-mouse Pyk2	Cell Signaling Technology	Cat# 3292, RRID: AB_2174097
anti-mouse Phospho-Pyk2 (Tyr402)	Cell Signaling Technology	Cat# 3291, RRID: AB_2300530
anti-mouse phospho-Tyrosine	Cell Signaling Technology	Cat# 9411, RRID: AB_331228
anti-Serotonin	Abcam	Cat# ab66047, RRID: AB_1142794
anti-mouse ChgA	Abcam	Cat# ab15160, RRID: AB_301704
anti-mouse KV1.2 (KCNA2)	Alomone Labs	Cat# APC-010, RRID: AB_2313792
anti-mouse Cd1d for PLA	Biolegend	Cat# 140802, RRID: AB_10639731
Bacterial strains		
Bacteroides fragilis	An et al[20]	N/A
Bacteroides fragilis ΔSPT	An et al[20]	N/A
Chemicals, peptides, and recombinant proteins		
Oxazolone (4-Ethoxymethylene-2-Phenyl-2-Oxazolin-5-One)	Sigma	Cat# 862207
α-Galcer	Avanti Polar Lipids	Cat# 867000P
Gsl-Bf717	An et al[20]	N/A
Sylgard-184	Ellsworth Adhesives	Cat# 4019862
Intesticult™ Organoid Growth Medium (Mouse)	Stemcell Technologies	Cat# 06005
Corning™ Matrigel™ Gfr Membrane Matrix	Corning	Cat# 356231
TrypLE	Thermo Fisher Scientific	Cat# 12604021
Carmine Red	Sigma	Cat# C1022–5G
1.5% Methylcellulose Solution	Aldon Corporation	Cat# MM0400
Thrombin	Sigma	Cat# T4648
Anti-CD3/CD28 Magnetic Beads	Thermo Fisher Scientific	Cat# 11456D

REAGENT or RESOURCE	SOURCE	IDENTIFIER
Recombinant Mouse IL-2	PeproTech	Cat# 212–12
Recombinant Mouse IL-7	R&D Systems	Cat# 407-ML-005/CF
Lipofectamine 3000	Thermo Fisher Scientific	Cat# L3000008
Celltrace™ Far Red	Thermo Fisher Scientific	Cat# C34572
Y-27632	Selleckchem	Cat# S1049
Fura-2 AM	Thermo Fisher Scientific	Cat# F1201
PF-431396	Sigma	Cat# PZ0185
mCPBG	Sigma	Cat# C144
Ondansetron	Tocris	Cat# 2891
Tstx-Kα	Alomone Labs	Cat# STT-360
Tetraethylammonium	Sigma	Cat# 86616
Fluoromount-G™, With DAPI	Thermo Fisher Scientific	Cat# 00–4959–52
Collagenase D	Sigma	Cat# 11088882001
4–12% Bis-Tris Gels	GenScript	Cat# M00653
Supersignal™ West Pico PLUS Chemiluminescent Substrate	Thermo Fisher Scientific	Cat# 34580
Protein A/G Magnetic Beads	Thermo Fisher Scientific	Cat# 88802
Critical commercial assays		
Serotonin ELISA kit	Enzo Life Sciences, Inc.	Cat# ADI-900–175
Duolink In Situ Orange Starter Kit Mouse/Rabbit	Sigma	Cat# DUO92102
iScript RT Supermix for RT-qPCR	Biorad	Cat# 1708841
RNeasy Plus Mini Kit	Qiagen	Cat# 74136
Experimental models: Cell lines		
BON-1 cells	Dr. Mark Hellmich	N/A
HEK293T	ATCC	Cat# CRL-3216
Experimental models: Organisms/strains		
Mouse: *Cd1d*$^{-/-}$	Jackson Laboratory	Cat# 003814
Mouse: *Traj18*$^{-/-}$	Jackson Laboratory	Cat# 030524
Mouse: *Va14* Tg	Jackson Laboratory	Cat# 014639
Mouse: *Cd11c*^{cre}	Jackson Laboratory	Cat# 008068
Mouse: *Rorc*^{cre}	Jackson Laboratory	Cat# 022791
Mouse: *Vil1*^{cre}	Jackson Laboratory	Cat# 021504
Mouse: PirtG^{CaMP3}	Kim et al[81]	N/A
Mouse: Tph1^{flox}	Yadav et al[82]	N/A
Mouse: Tph1^{CFP}	Li et al[83]	N/A
Mouse: Cd1d1^{flox}	MMRRC	Cat# 043942
Mouse: *Chga*^{creER}	EMMA	Cat# 09574
Oligonucleotides		
Tph1 - forward 5' ATGGATCCGAACTTGACGCC	IDT	N/A

REAGENT or RESOURCE	SOURCE	IDENTIFIER
Tph1 - reverse 5' GGGTCCCCATGTTTGTAGTTC	IDT	N/A
Slc6a4 - forward 5' GCGACGTGAAGGAAATGCTGG	IDT	N/A
Slc6a4 - reverse 5' ATAGGGATGCAGATGACAGACG	IDT	N/A
Slc18a1 - forward 5' TCTCTGGCACCTATGCCCT	IDT	N/A
Slc18a1 - reverse 5' TGCCCACAAATTCATACATCACA	IDT	N/A
Ddc - forward 5' TAGCTGACTATCTGGATGGCAT	IDT	N/A
Ddc - reverse 5' GTCCTCGTATGTTTCTGGCTC	IDT	N/A
Maoa - forward 5' GCCCAGTATCACAGGCCAC	IDT	N/A
Maoa - reverse 5' GTCCCACATAAGCTCCACCA	IDT	N/A
Maob - forward 5' ATGAGCAACAAAAGCGATGTGA	IDT	N/A
Maob - reverse 5' TCCTAATTGTGTAAGTCCTGCCT	IDT	N/A
Actb - forward 5' GGCTGTATTCCCCTCCATCG	IDT	N/A
Actb - reverse 5' CCAGTTGGTAACAATGCCATGT	IDT	N/A
Recombinant DNA		
pLV-EF1a-IRES-mCherry	Addgene	Cat# 85132
psPAX2	Addgene	Cat# 12260
pMD2.G	Addgene	Cat# 12259
pcDNA3.1–5HT3R-IRES-mCherry	This paper	N/A
Mouse Cd1d1 cDNA clone	Sino Biological	Cat# MG50188-M
Software and algorithms		
GraphPad Prism version 8	Graphpad Software	https://www.graphpad.com
FlowJo	TreeStar	https://www.flowjo.com/
ImageJ	ImageJ	https://imagej.net/Welcome
pClamp 10.6	Molecular Devices	https://www.moleculardevices.com/products/axon-patch-clampsystem/acquisition-andanalysissoftware/pclampsoftware-suite#gref
LabChart	AD instruments	https://www.adinstruments.com/products/labchart
NIS-elements	Nikon	https://www.microscope.healthcare.nikon.com/products/software/nis-elements